International Journal of Heat and Mass Transfer 203 (2023) 123760

Contents lists available at ScienceDirect

International Journal of Heat and Mass Transfer

journal homepage: www.elsevier.com/locate/hmt

Dynamic melting in an open enclosure supported by a partial layer of metal foam: A fast thermal charging approach

Mehdi Ghalambaz[a,b], Mutabe Aljaghtham[c], Ali J. Chamkha[d], Abdelkader Abdullah[c,e], Umar Alqsair[c], Mohammad Ghalambaz[f,*]

[a] Institute of Research and Development, Duy Tan University, Da Nang 550000, Vietnam
[b] Faculty of Electrical – Electronic Engineering, Duy Tan University, Da Nang 550000, Vietnam
[c] Department of Mechanical Engineering, College of Engineering in Al-Kharj, Prince Sattam Bin Abdulaziz University, Al-Kharj 11942, Saudi Arabia
[d] Faculty of Engineering, Kuwait College of Science and Technology, Doha District, Kuwait
[e] Mechanical Power Engineering Department, Faculty of Engineering, Tanta University, Tanta 31521, Egypt
[f] Laboratory on Convective Heat and Mass Transfer, Tomsk State University, 634045 Tomsk, Russia

ARTICLE INFO

Article history:
Received 12 October 2022
Revised 2 December 2022
Accepted 7 December 2022
Available online 25 December 2022

Keywords:
Dynamic phase change
Porous medium
Latent heat thermal energy storage
Forced convection melting heat transfer

ABSTRACT

A new design of fast charging latent heat thermal energy storage (dynamic melting) is proposed to further reduce the charging time. The proposed new design benefits from a stream of pressurized and heated liquid PCM entering and leaving the storage unit. Two layers of metal foam were also added to accelerate the thermal charging process further. The governing equations for the flow and heat transfer with phase change were introduced as partial differential equations and integrated using the finite element method. The impact of the porosity of foam layers, the foam ratio, and the geometrical placement of layers was investigated in the proposed design. The mounting location of a horizontal foam layer was not much important. Interestingly, it was found that a metal foam with high porosity produces a short thermal charging time. It was since the most important parameter in controlling the thermal charging time was forming a liquid PCM film between the inlet and outlet ports of the enclosure. Such as liquid film allows a passage for the pressurized and heated liquid PCM enters the enclosure and accelerates the melting process by a mixed convection mechanism. A full melting could be achieved in about 2.5 h in a 16-inch diameter enclosure.

1. Introduction

In addition to environmental pollution, fair prices, greenhouse gas emissions, and global warming, scientists have long been concerned about sustainable supply. A viable alternative to fossil fuels is undoubtedly using renewable energy sources. Growing inequalities between energy demand and supply and massive quantities of energy needed raise concerns. Storage of surplus energy is a viable solution. These systems can be electrical, mechanical, or thermal. Latent heat and sensible energy storage are the two most common types of thermal energy storage (TES) [1]. The stored heat in Latent Heat Thermal Energy Storage (LHTES) system is derived from the phase change enthalpy or specific latent heat due to the phase transition at a certain temperature [2,3]. An essential component of TES systems is a phase change material (PCM). A key drawback of PCMs is their low thermal conductivity, which limits them from being widely used. These materials, however, have piqued the interest of researchers due to their numerous applications. Substantial studies have been conducted to address this issue and improve the thermophysical properties of these materials [4–6]. Using metal foam [7,8], fins [9], carbon nanotubes [10], and nanoparticles [11] can improve PCM's thermal conductivity and heat transfer rate.

Metal foam (MF) has a low density, a large specific surface area, a low complex permittivity, and a high thermal conductivity [12]. Using MF in TES systems may help to address PCMs' poor thermal conductivity [13,14]. It was discovered by Esapour et al. [15] that the addition of MF improves temperature distribution and improves thermal conductivity. TES unit proposed by Yang et al. [16] utilized MF and showed that reducing the melt time by 88.6 percent could significantly improve the TES. The impact of heat generation [17], pore density [18], and nanoparticles [19] have been addressed in the heat transfer of PCMs in recent investigations.

Wang et al. [20] examined copper foams' charging/discharging behaviors in a vertical LHTES tube with radial gradient porosity. The development of thin-film MFPCM systems has recently

* Corresponding author at: Laboratory on Convective Heat and Mass Transfer, Tomsk State University, 634045 Tomsk, Russia.
E-mail address: m.ghalambaz@gmail.com (M. Ghalambaz).

https://doi.org/10.1016/j.ijheatmasstransfer.2022.123760
0017-9310/

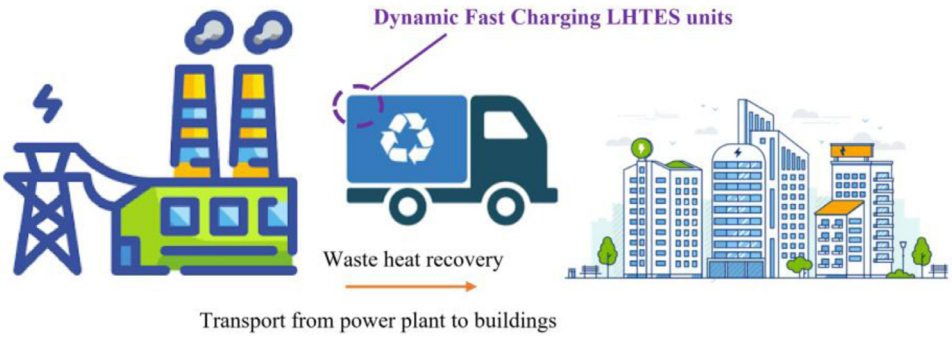

Fig. 1. A schematic of the dynamic fast charging LHTES unit application.

been applied to cooling various electronic components, including GPUs, CPUs, laptops, LCDs, and tablets [21]. Joshi and Rathod [22] and Zhu et al. [23] suggested MF filling ratios of 1/2 [22] for an enclosure heated from the side and 2/3 [23] when heated from the bottom. Li et al. [24] indicated that the heat transfer rate of MFPCM is approximately 11 times greater than that of pure PCM. However, volume density of new TES is 2.2–2.5 times greater than traditional. Ferfera and Madani [25] investigated experimentally and computationally the heat storage capacity of composite Cu/Ni foams-PCMs with different pore densities and porosities. The composite PCMs' thermal diffusivity and conductivity were discovered to have increased by 35 and 6 times, respectively.

While specific methods for enhancing heat transfer have been highly successful, they are invasive since only a tiny amount of PCM may be placed within the Latent Heat TES (LHTES) set. As a result, the PCM volume to LHTES system volume ratio decreases, as does the energy storage capacity. Recent studies show that the porosity and PPIs [26,27], hyper-gravity [28], or variable morphologies [29] impact the melting rate. Besides, a comparison between utilized techniques shows that the metal foams can better enhance the melting heat transfer than for instance, nanoparticles [30,31].

Some heat transfer techniques that do not need invasiveness augmentation, such as dynamic PCM systems, direct contact PCM structures, and PCM slurries, were investigated [32,33]. During the phase transition, dynamic PCM systems move or agitate the PCM. They may be divided into four major categories. The first LHTES system strategy is to include ultrasonic vibrations in the system, which improves system performance by avoiding the formation of solid PCM layers in the subcooled liquid PCM [34,35]. The second approach, a twin-screw heat exchanger, entails spinning a heat exchanger's heat transfer surface helicoidally during charging and discharging operations [36]. The PCM flux, which is a transport tube that carries PCM across a heated surface, is the third idea. The fourth option is dynamic melting. Liquid PCM is recirculated through an external mechanism to control the flow and transfer of heat during melting.

Continuous mixing of the PCM with motion increases overall heat transfer and system efficiency by minimizing charging time and increasing forced convection. This approach also reduces PCM deterioration and phase segregation by maintaining a high packing factor [37]. Tay et al. [38] evaluated the PCM dynamic melting process of a tube-in-tank theoretically and physically, capturing improvements in melting time, heat transfer, and efficacy. In another study, Tay et al. [39] experimentally tested the dynamic melting of a tube-in-tank configuration. In their test, the liquid PCM flows as HTF liquid in copper tubes and could enter the LHTES tank and interact with the remaining solid PCM in the unit. The flow of liquid PCM in the storage unit could shorten the thermal charging time. Thus, the authors concluded from the experiments that dynamic melting could be considered an effective technique for promoting

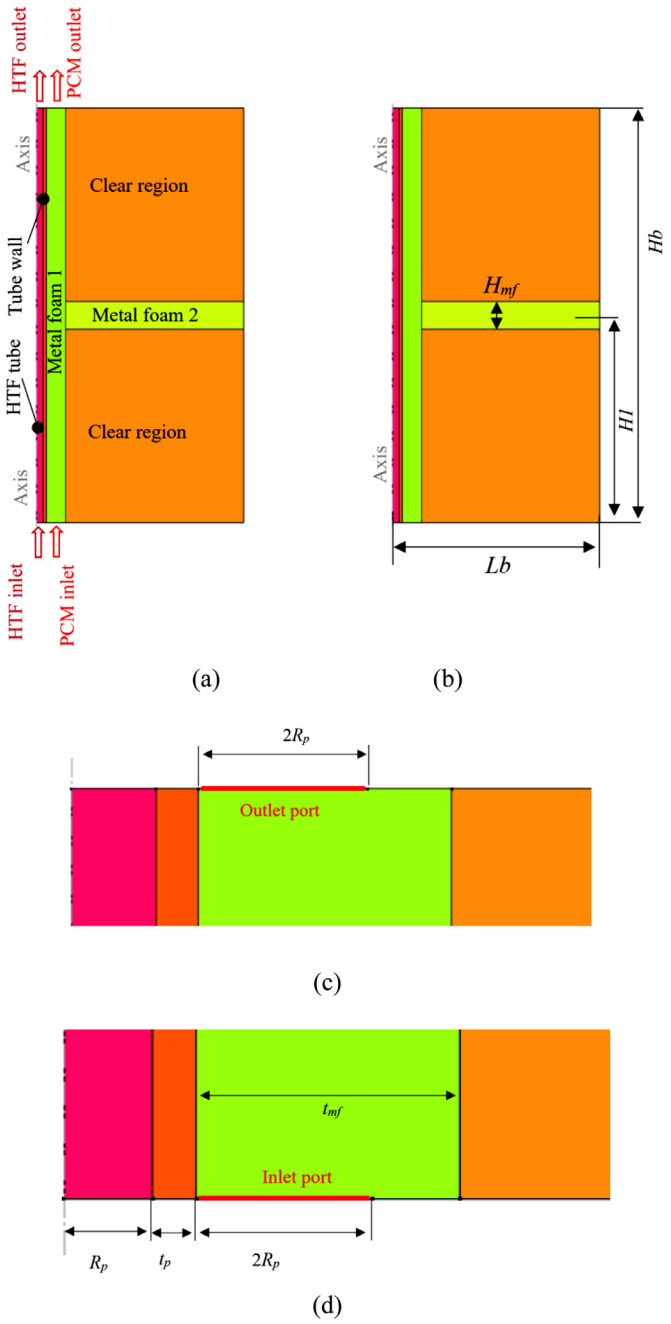

Fig. 2. Schematic diagram of the physical model of a fast-charging LHTES unit. (a) a general view of the model, (b) geometrical details, (c) the magnified top section geometrical details, (d) the magnified bottom section geometrical details.

Table 1
Thermophysical properties of the Coconut oil and the nano additives [51,52].

Properties	Coconut oil (measured)		HTF (water at T_{in})	Copper pipe (thick wall)	Copper foam
	Solid (15 °C)	Liquid (32 °C)			
ρ_{PCM} (kgm^{-1})	920	914 ± 0.11%	993.73	8900	8900
μ_{PCM} (Nsm^{-2})	-	0.0326 ± 3%	0.705 × 10^{-3}	-	-
C_p (JkgK^{-1})	3750	2010 ± 0.2%	4178	386	386
k (Wm^{-1}K^{-1})	0.228	0.166 ± 1.2%	0.623	380	380
h_f (kJkg^{-1})		103 ± 1%		-	-
Pr		394.73 ± 3.2%		-	-
T_{me} (ΔT_{me})	24 °C (±1°C)			-	-

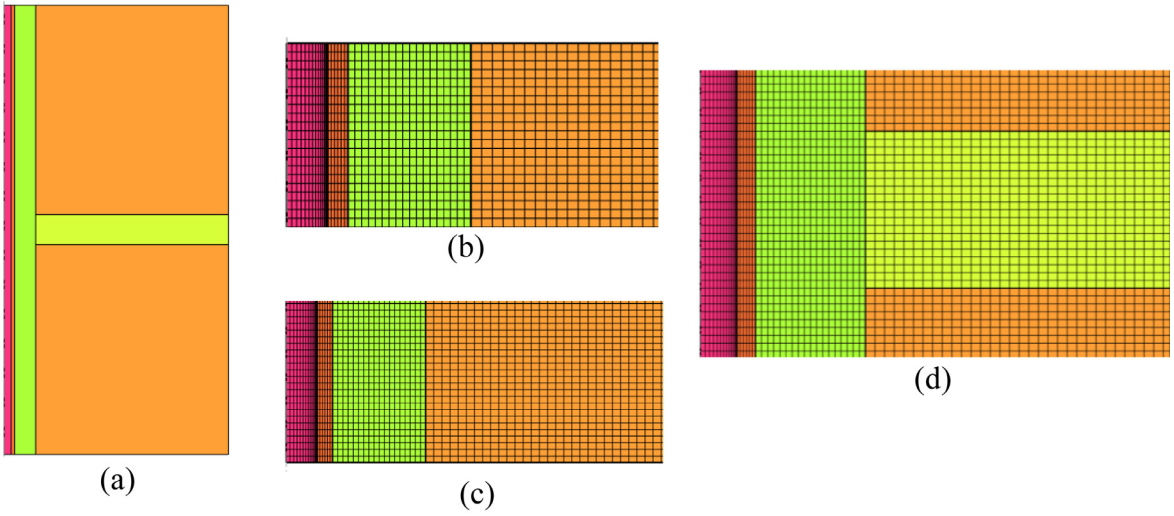

Fig. 3. Views of the mesh with N=3. (a) general view; (b) Top region; (c) bottom region; (d) the extended foam region.

Table 2
The range and levels of control parameters.

Factors	Description	Range	Level 1	Level 2	Level 3	Level 4
A	ε_1 Porosity	0.85-0.975	0.825	0.875	0.925	0.975
B	ε_2 Porosity	0.85-0.975	0.825	0.875	0.925	0.975
C	t_{mf}/ R_p The metal foam ratio wave number	2 – 5	2	3	4	5
D	NL The height ratio of fin	-4 – 2	-4	-2	0	2

heat transfer in LHTES systems. Later, Gasia et al. [40] empirically tested the thermal charging of a shell-tube shape LHTES unit with dynamic melting. In their design, a pump circulates the liquid PCM in the shell side. The experiments show a 65.3% save in the melting time.

Even though the mentioned studies revealed that MF improves the heat transfer performance of PCMs, each approach has significant drawbacks. MFs do not contribute to latent energy storage since they do not change phase, hindering normal convection flow. MF occupies PCM space and adds weight to the machine. A partial-filling technique was recently designed to completely utilize the power of natural convection and heat transfer enhancement [41]. The research investigates the effects of using a layer of metal foam and high-temperature PCM entering the tank on energy storage performances.

The literature review shows only a few publications on the dynamic melting of LHTES units [37–40], which are primarily experimental investigations. The experiments show a significant acceleration in the melting process and a reduction in the charging time. Thus, the current study aims to simulate dynamic melting better to highlight the contributing mechanism during the melting process. The impact of using metal foam layers and their geometrical configurations on the thermal charging time was addressed for the first time.

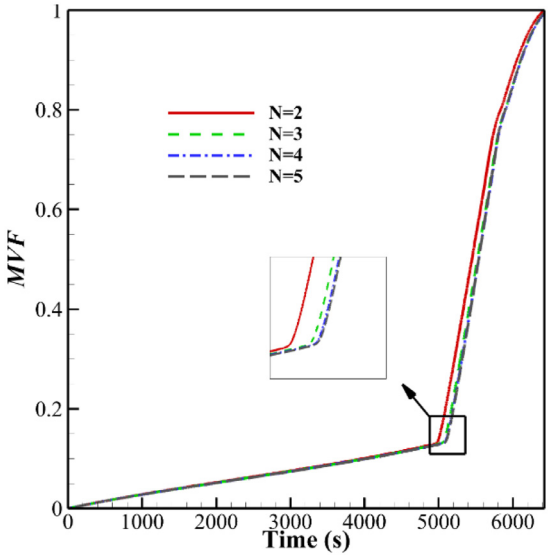

Fig. 4. Grid independency process performed for melting volume fraction, the total energy stored, PCM outlet average velocity from zero up to 8000 s.

Table 3
Taguchi orthogonal table (L16) for design variables and optimization goal.

Case	A	B	C	D	MVF = 0.95			S/N Ratio
	ε_1	ε_2	t_{mf}/R_p	NL	Time (s)	ES (kJ/kg)	P(kW/kg)	
1	0.825	0.825	2	-4	12,463	49.9	4.00	-81.91
2	0.825	0.875	3	-2	12,986	75.8	5.83	-82.27
3	0.825	0.925	4	0	12,873	111.4	8.65	-82.19
4	0.825	0.975	5	2	7378	154.2	20.90	-77.36
5	0.875	0.825	3	0	11,854	51.4	4.34	-81.48
6	0.875	0.875	2	2	14,798	80.5	5.44	-83.40
7	0.875	0.925	5	-4	12,074	113.6	9.41	-81.64
8	0.875	0.975	4	-2	6658	155.4	23.34	-76.47
9	0.925	0.825	4	2	11,042	73.9	6.70	-80.86
10	0.925	0.875	5	0	11,119	91.8	8.26	-80.92
11	0.925	0.925	2	-2	13,237	115.2	8.70	-82.44
12	0.925	0.975	3	-4	5406	157.5	29.13	-74.66
13	0.975	0.825	5	-2	3341	81.7	24.46	-70.48
14	0.975	0.875	4	-4	3936	97.1	24.66	-71.90
15	0.975	0.925	3	2	4404	120.3	27.32	-72.88
16	0.975	0.975	2	0	2849	161.1	56.54	-69.09
17	0.975	0.975	5	-4	2376	161.5	68.01	Optimum

Table 4
Further investigation on the impact of design parameters.

Case	Parameter investigation	A ε_1	B ε_2	C T_{mf}/R_p	D NL
0	Default case	0.875	0.875	3	0
1	$_1\varepsilon$	0.825	0.875	3	0
2		0.925	0.875	3	0
3		0.975	0.875	3	0
4	ε_2	0.875	0.825	3	0
5		0.875	0.925	3	0
6		0.875	0.975	3	0
7	T_{mf}/Rp	0.875	0.875	2	0
8		0.875	0.875	4	0
9		0.875	0.875	5	0
10	NL	0.825	0.975	3	-4
11		0.825	0.975	3	-2
12		0.825	0.975	3	0
13		0.825	0.975	3	2

2. Model description and formulation

2.1. Model description

A new design of PCM enclosures with open ports for a flowing stream of liquid PCM was introduced. The proposed fast charging Latent Heat Thermal Energy Storage (LHTES) unit could be used for waste heat recovery from power plants. A stuck of fast charging LHTES units, loaded in trucks, absorbs low-quality excess heat of a power plant at the plant site. Then, the charged units could be transported to building sites to be used for building heating, as shown in Fig. 1.

Each LHTES unit is an enclosure filled with metal foam and PCM. The enclosure is an annuli design with a heated tube in the center, as illustrated in Fig. 2. There is a flow of heated water as the heat transfer fluid (HTF) in the center tube. The PCM with a fusion temperature T_f is filled in the annuli space. The bottom and top of the annuli space are open so a pressurized stream liquid PCM can enter the annuli space from the bottom and leave the system at the top. There is a metal foam layer with porosity (ε_1) and permeability (K_1) over the HTF tube. Besides, there is a layer of metal foam with a porosity (ε_2) and permeability (K_2), which is extended into the annuli space. Fig. 2 shows a general view of the design and its geometrical details. The mounting location of the extended foam layer can be introduced by NL=$H1/Hb$. Since both foam layers are made of same material, they can be welded or machined at once.

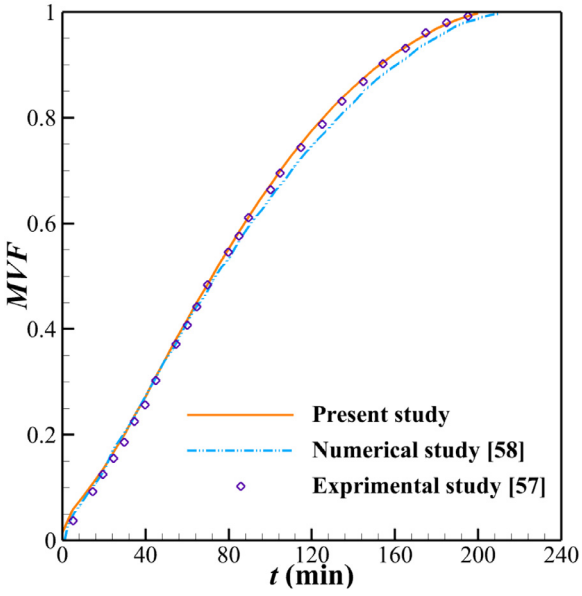

Fig. 5. The simulation results of the current model with the literature's theoretical [58] and measurements [57] data.

Initially, the PCM in the system is in the super cold state ($T_0 < T_f$), and a flow of heated liquid PCM cannot enter the system. However, a stream of heated water ($T_h > T_f$) in the HTF tube is possible. The heat transfer through the tub's wall melts a layer of solid PCM inside the system and creates a thin film of liquid PCM, allowing a stream of liquid PCM enters the system from the bottom port. The top port is exposed to a relative pressure of zero, while the bottom port is maintained at a high temperature (T_h) and pressure (P_{in}). The stream of the liquid PCM through the annuli space is expected to increase the heat transfer rate and accelerate the charging process (reducing the melting time) significantly. Indeed, a high-pressure inlet liquid PCM induces mixed convection flow and boosts the convection heat transfer mechanism in the enclosure. As a result, an enhanced heat transfer rate at the melting front can be expected. The extended layer with porosity ε_2 tends to uniform the fluid flow in the enclosure and divert it away from the HTF tube toward the shell regions of the enclosure. The diverted hot inlet flow may better melt the solid regions next to the enclosure shell. The current study aims to analyze the above-explained model of thermal energy storage.

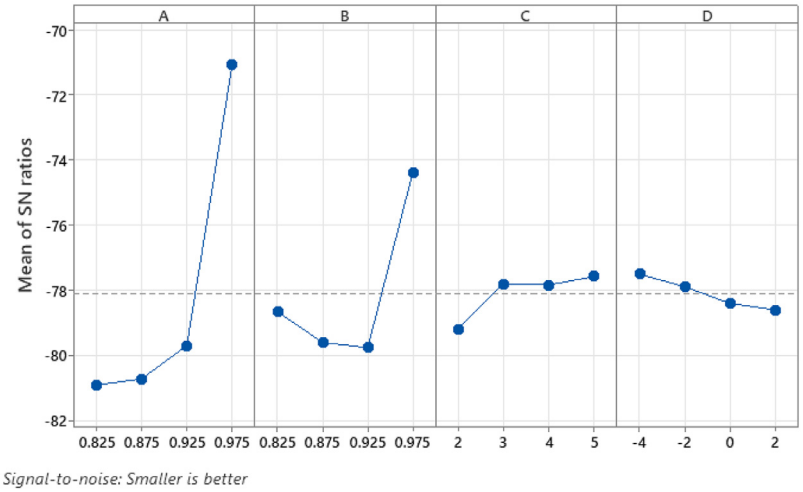

Fig. 6. The computed S/N ratios for each design parameter. The maximum S/N ratio was selected based on the Taguchi method, which are ε_1=0.975, ε_2=0.975, t_{mf}/R_p=5, and NL=-4.

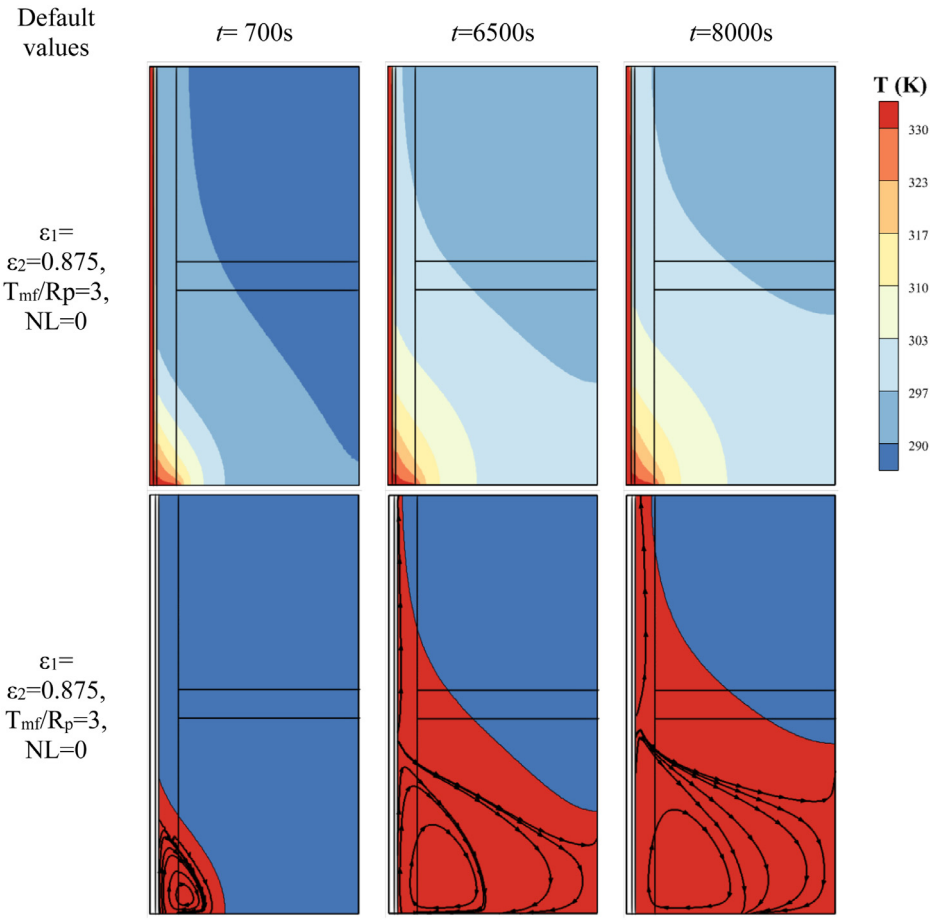

Fig. 7. Isotherm (top row) and streamlines (bottom row) for default values of the parameters.

2.2. Mathematical formulation

The governing equations for the explained model include the forced convection flow and heat transfer in the HTF tube, the conjugate heat transfer in the tube wall, and the mixed convection heat transfer with phase change in the annuli space. The Darcy-Brinkmann model governs the flow and heat transfer in the composite PCM-metal foam regions.

2.2.1. Governing equations for heat transfer fluid (HTF)

The governing equations for conservation of mass momentum for HTF flow can be explained as [42,43]:

The conservation of mass:

$$\frac{1}{r}\frac{\partial(ru)}{\partial r}+\frac{\partial w}{\partial z}=0 \tag{1}$$

where u and w are the velocity components in horizontal (r) and vertical directions (z).

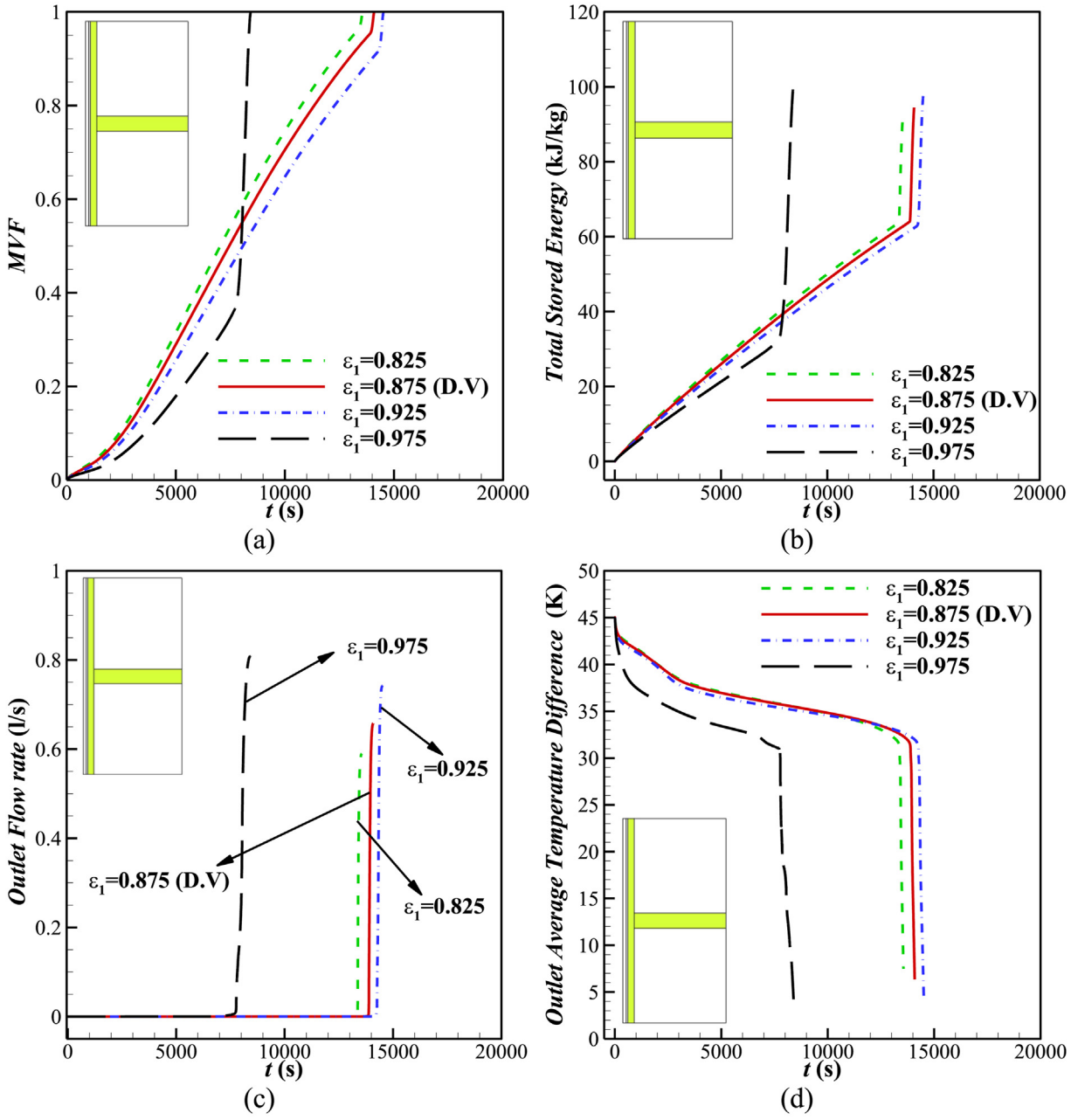

Fig. 8. Effect of porosity parameter in the region 1 (ε_1) on the (a) melting volume fraction, (b) total stored energy, (c) outlet flow range, and (d) outlet average temperature.

The conservation of momentum is explained as:

$$\rho_{HTF}\left(\frac{\partial u}{\partial t}+u\frac{\partial u}{\partial r}+w\frac{\partial u}{\partial z}\right)=-\frac{\partial p}{\partial r}+\frac{\mu_{HTF}}{r}\frac{\partial}{\partial r}\left(r\frac{\partial u}{\partial r}\right)-\frac{\mu_{HTF}u}{r^2}+\mu_{HTF}\frac{\partial^2 u}{\partial z^2} \quad (2)$$

$$\rho_{HTF}\left(\frac{\partial w}{\partial t}+u\frac{\partial w}{\partial r}+w\frac{\partial w}{\partial z}\right)=-\frac{\partial p}{\partial z}+\frac{\mu_{HTF}}{r}\frac{\partial}{\partial r}\left(r\frac{\partial w}{\partial r}\right)+\mu_{HTF}\frac{\partial^2 w}{\partial z^2} \quad (3)$$

where p is the pressure field. The symbols ρ and μ denote the density and dynamic viscosity. The subscript HTF indicates the HTF fluid, which here is water.

The conservation of the energy in the HTF is explained by:

$$(\rho C_p)_{HTF}\left(\frac{\partial T}{\partial t}+u\frac{\partial T}{\partial r}+w\frac{\partial T}{\partial z}\right)=\frac{1}{r}\frac{\partial}{\partial r}\left(k_{HTF}r\frac{\partial T}{\partial r}\right)+\frac{\partial}{\partial z}\left(k_{HTF}\frac{\partial T}{\partial z}\right) \quad (4)$$

where T is the temperature field, and C_p and k are the specific heat capacity at constant pressure and the thermal conductivity.

2.2.2. Governing equations for the tube wall

The enegy conservation equation for copper pipe as a solid intermediate thick wall is explaned as [43,44]:

$$(\rho c_p)_w\frac{\partial T}{\partial t}=k_w\left(\frac{1}{r}\frac{\partial}{\partial r}\left(\frac{\partial T}{\partial r}\right)+\frac{\partial^2 T}{\partial z^2}\right) \quad (5)$$

where the subscript w denotes the wall.

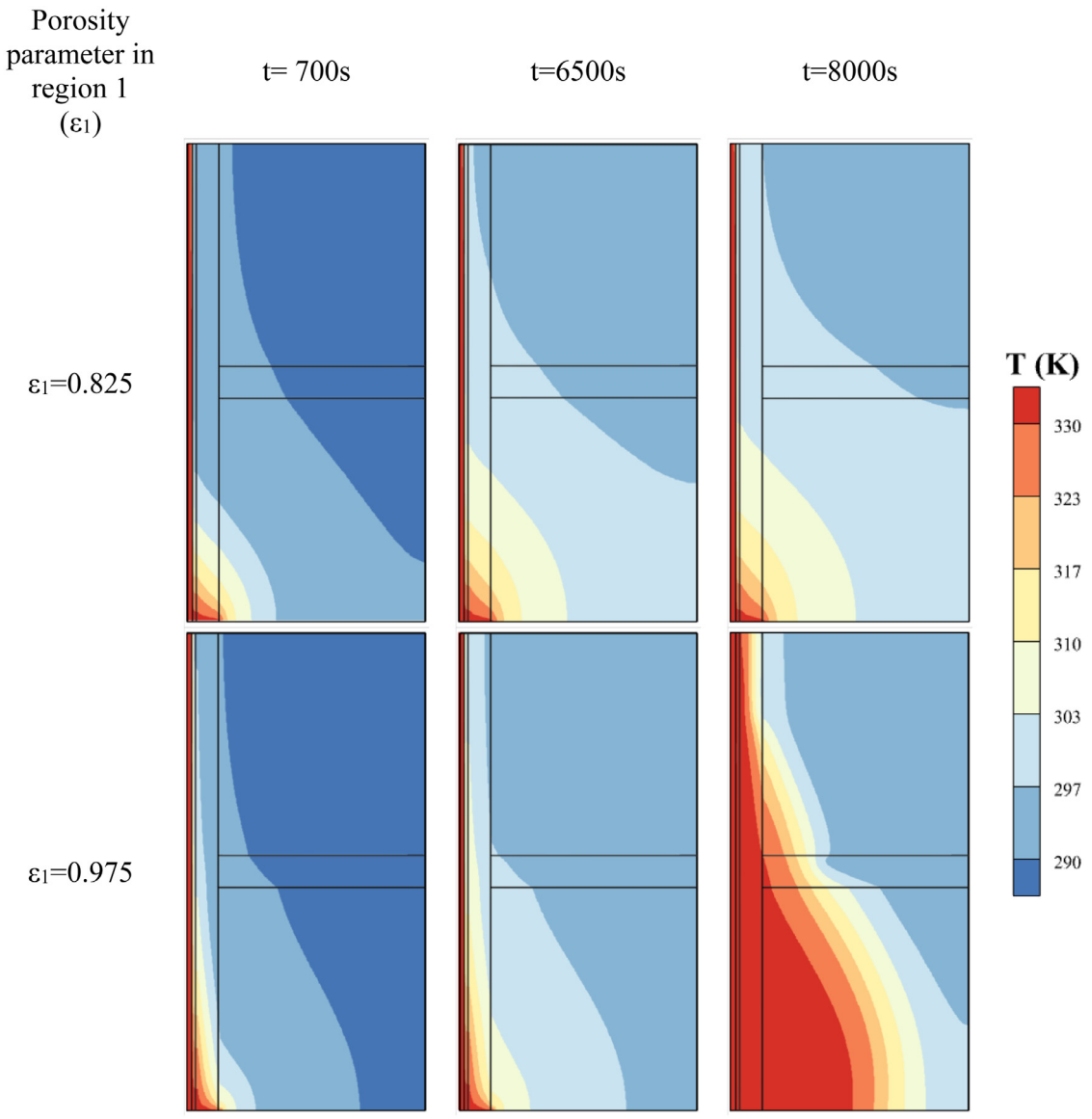

Fig. 9. Effect of porosity parameter in the region 1 (ε_1) on the contours of isotherm ε_1=0.825 (top row) and ε_1=0.975 (bottom row).

2.2.3. Governing equations for annuli space

The conservation of mass is introduced as [42,43,45]:

$$\frac{1}{r}\frac{\partial(ru)}{\partial r}+\frac{\partial w}{\partial z}=0 \tag{6}$$

The momentum equation in horizontal and vertical directions are

$$\frac{\rho_{PCM}}{\varepsilon}\frac{\partial u}{\partial t}+\frac{\rho_{PCM}}{\varepsilon^2}\left(u\frac{\partial u}{\partial r}+w\frac{\partial u}{\partial z}\right)=-\frac{\partial P}{\partial r}$$
$$+\frac{\mu_{PCM}}{\varepsilon}\left(\frac{1}{r}\frac{\partial}{\partial r}\left(r\frac{\partial u}{\partial r}\right)-\frac{u}{r^2}+\frac{\partial^2 u}{\partial z^2}\right)-\frac{\mu_{PCM}}{K}u-s(T)u \tag{7}$$

$$\frac{\rho_{PCM}}{\varepsilon}\frac{\partial w}{\partial t}+\frac{\rho_{PCM}}{\varepsilon^2}\left(u\frac{\partial w}{\partial r}+w\frac{\partial w}{\partial z}\right)=-\frac{\partial P}{\partial z}$$
$$+\frac{\mu_{PCM}}{\varepsilon}\left(\frac{1}{r}\frac{\partial}{\partial r}\left(r\frac{\partial w}{\partial r}\right)+\frac{\partial^2 w}{\partial z^2}\right)$$
$$-\frac{\mu_{PCM}}{K}w-s(T)w+\rho_{PCM}g\beta_{PCM}\left(T-T_f\right) \tag{8}$$

where the subscript PCM indicates the phase change material. Here, ε and K are the porosity and thermal conductivity of the metal foam. The porosity is unity (ε=1), and permeability tends to infinity in the clear regions. In the metal foam, the porosity and permeability tend to the corresponding values of the metal foam. The symbols β and g are also the thermal expansion coefficient and the gravity acceleration. $S(T)$ is a sink term that controls the velocity in the solid and liquid regions and was explained later.

The conservation of energy is explained as [42,43,45]:

$$(\rho c_p)_{eff}\frac{\partial T}{\partial t}+(\rho c_p)_{PCM,l}\left(u\frac{\partial T}{\partial r}+w\frac{\partial T}{\partial z}\right)$$
$$+\varepsilon\rho_{PCM,l}L_f\frac{\partial\omega(T)}{\partial t}=k_{eff}\left(\frac{1}{r}\frac{\partial}{\partial r}\left(\frac{\partial T}{\partial r}\right)+\frac{\partial^2 T}{\partial z^2}\right) \tag{9}$$

where L_f is the latent heat of fusion, and ω(T) is the melting fraction. The melting fraction can be changed between zero (fully solid) and one (fully liquid) and was described mathematically later. The subscript eff denoted the effective properties of the composite metal foam and PCM. The permeability of the metal foam is

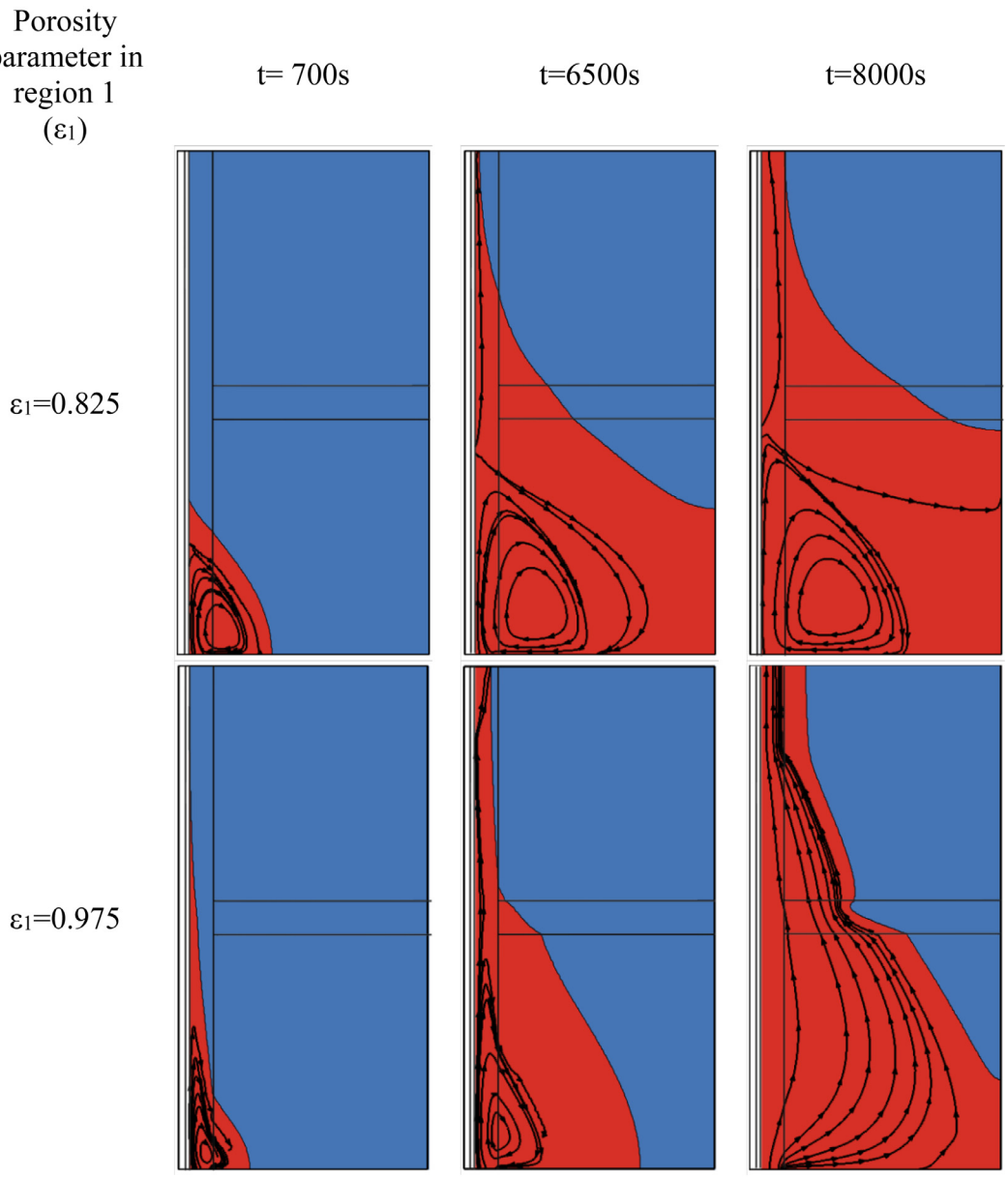

Fig. 10. Effect of porosity parameter in the region 1 (ε_1) on the streamlines; ε_1=0.825 (top row) and ε_1=0.975 (bottom row).

computed using the following equation [46]:

$$K = d_p^2 \frac{73\times10^{-5}}{(1-\varepsilon)^{0.224}}\left(d_l d_p^{-1}\right)^{-1.11},\ \left(d_l d_p^{-1}\right) = 1.18\left(\frac{1-\varepsilon}{3\pi}\right)^{0.5}$$
$$[1-\exp\left(-(1-\varepsilon)/0.04\right)]^{-1},\ d_p = 254\times10^{-4}\omega^{-1}(PPI) \quad (10)$$

with a fixed pore density of 5 PPI.

The sink term s(T) is also introduced as $s(T) = A_{mush}\frac{1-2\omega(T)+\omega^2(T)}{\lambda+\omega^3(T)}$, in which

$$\omega(T) = \begin{cases} 0 & T < T_{me} - \Delta T_{me}/2 \\ \dfrac{T-T_{me}}{\Delta T_{me}} + \dfrac{1}{2} & T_{me} - \Delta T_{me}/2 < T < T_{me} + \Delta T_{me}/2 \\ 1 & T > T_{me} + \Delta T_{me}/2 \end{cases} \quad (11)$$

where A_{mush} is adopted as 10^6 kg/(m^{3}s) in clear flow and 10^{11} kg/(m^{3}s) in metal foam region. Moreover, λ=10^{-3} and ΔT_{me} is the melting range.

For effective thermophysical properties [47,48]:

$$(\rho C_p)_{PCM} = \omega(T)(\rho C_p)_{PCM,l} + (1-\omega(T))(\rho C_p)_{PCM,s} \quad (12)$$

where the subscripts l and s denote the solid and liquid phases of the PCMs.

$$(\rho C_p)_{eff,PCM} = \varepsilon(\rho C_p)_{PCM} + (1-\varepsilon)(\rho C_p)_{porous} \quad (13)$$

where the subscript porous indicates the metal foam property. The thermal conductivity of the PCM is computed using the melting volume fractions as:

$$k_{PCM} = \omega(T)k_l + (1-\omega(T))k_s \quad (14)$$

The effective thermal conductivity of composite porous metal foams is evaluated as [49,50]:

$$k_{eff} = \frac{[k_{PCM} + \pi(\sqrt{\chi}-\chi)\Delta k][k_{PCM} + (\chi\pi)\Delta k]}{k_{PCM} + \left[\frac{4}{3}\sqrt{\chi}(1-\varepsilon) + \pi\sqrt{\chi} - (1-\varepsilon)\right]\Delta k} \quad (15)$$

in which,

$$\chi = \frac{1-\varepsilon}{3\pi},\ \Delta k = k_{porous} - k_{PCM} \quad (16)$$

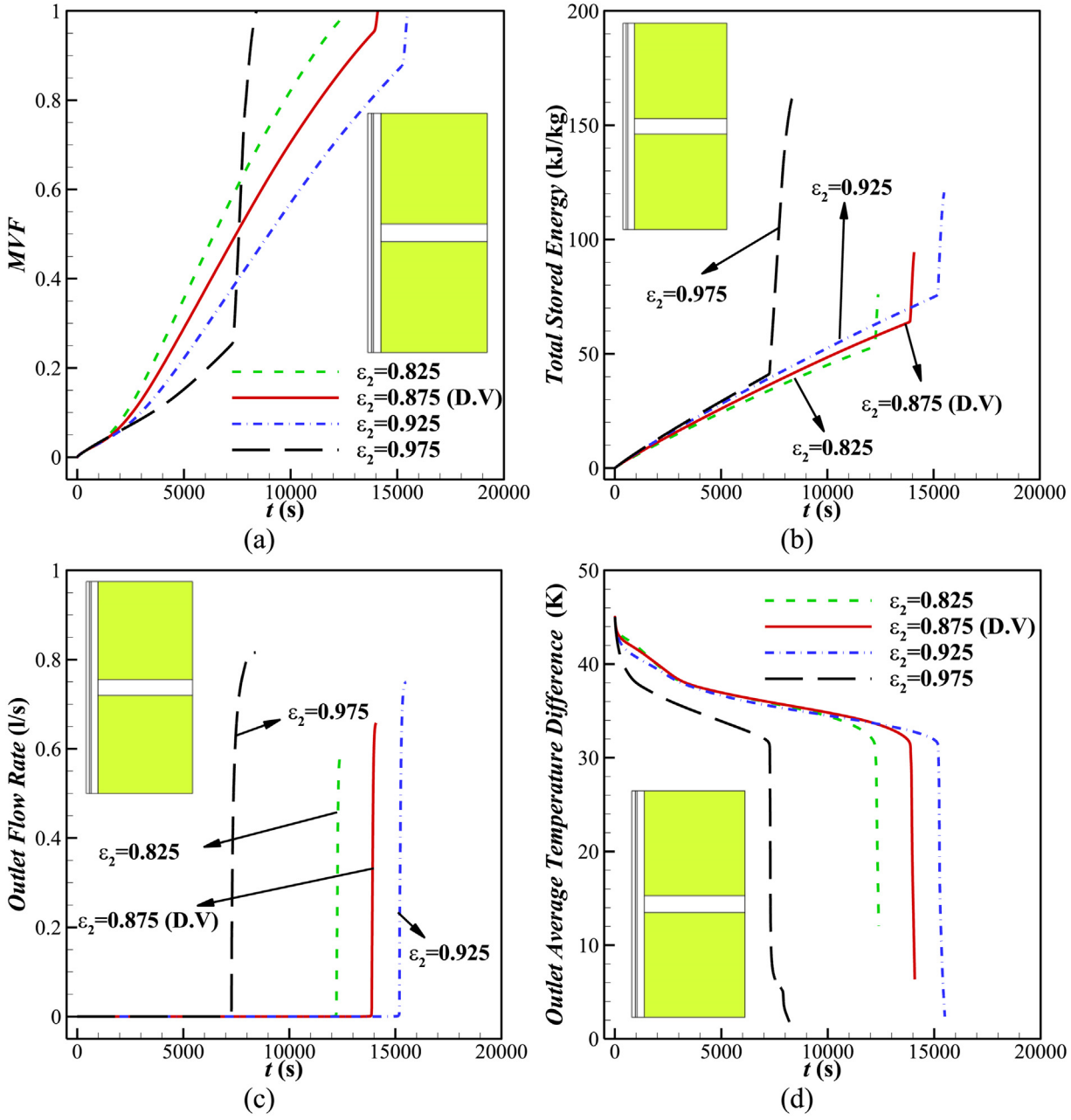

Fig. 11. Effect of porosity parameter in the region 2 (ε_2) on the (a) melting volume fraction, (b) total stored energy, (c) outlet flow range, and (d) outlet average temperature.

The thermophysical properties of metal foam, HTF, tube wall, and PCM are summarized in Table 1.

2.3. Controlling boundary and initial conditions

The HTF is injected with the temperature of $T_{in,HTF,}$ and velocity of $w_{in,HTF}$.

$$T|_{HTF} = T_h,\ u|_{HTF} = 0,\ w|_{HTF} = w_{in,HTF} \tag{16}$$

At the outlet of the HTF tube, the developed convective flow is considered to be established.

$$u|_{HTF} = 0,\ P|_{HTF} = 0,\ \left.\frac{\partial T}{\partial z}\right|_{HTF} = 0 \tag{18}$$

The injected PCM in the bottom to up direction can be written as:

$$P|_{PCM} = P_{in,PCM} and\ T|_{PCM} = T_h \tag{19}$$

and at the outlet, it is expected:

$$P|_{PCM} = 0,\ and\ \left.\frac{\partial T}{\partial z}\right|_{PCM} = 0 \tag{20}$$

The perimeter wall of the enclosure is well insulated, and hence, the boundary conditions at the outer wall are:

$$u|_{PCM} = w|_{PCM} = 0,\ \left.\frac{\partial T}{\partial r}\right|_{PCM} = 0 \tag{21}$$

At the upper and lower surfaces of the PCM enclosure, boundary conditions can be defined as the following:

$$u|_{PCM} = w|_{PCM} = 0,\ \left.\frac{\partial T}{\partial z}\right|_{PCM} = 0 \tag{22}$$

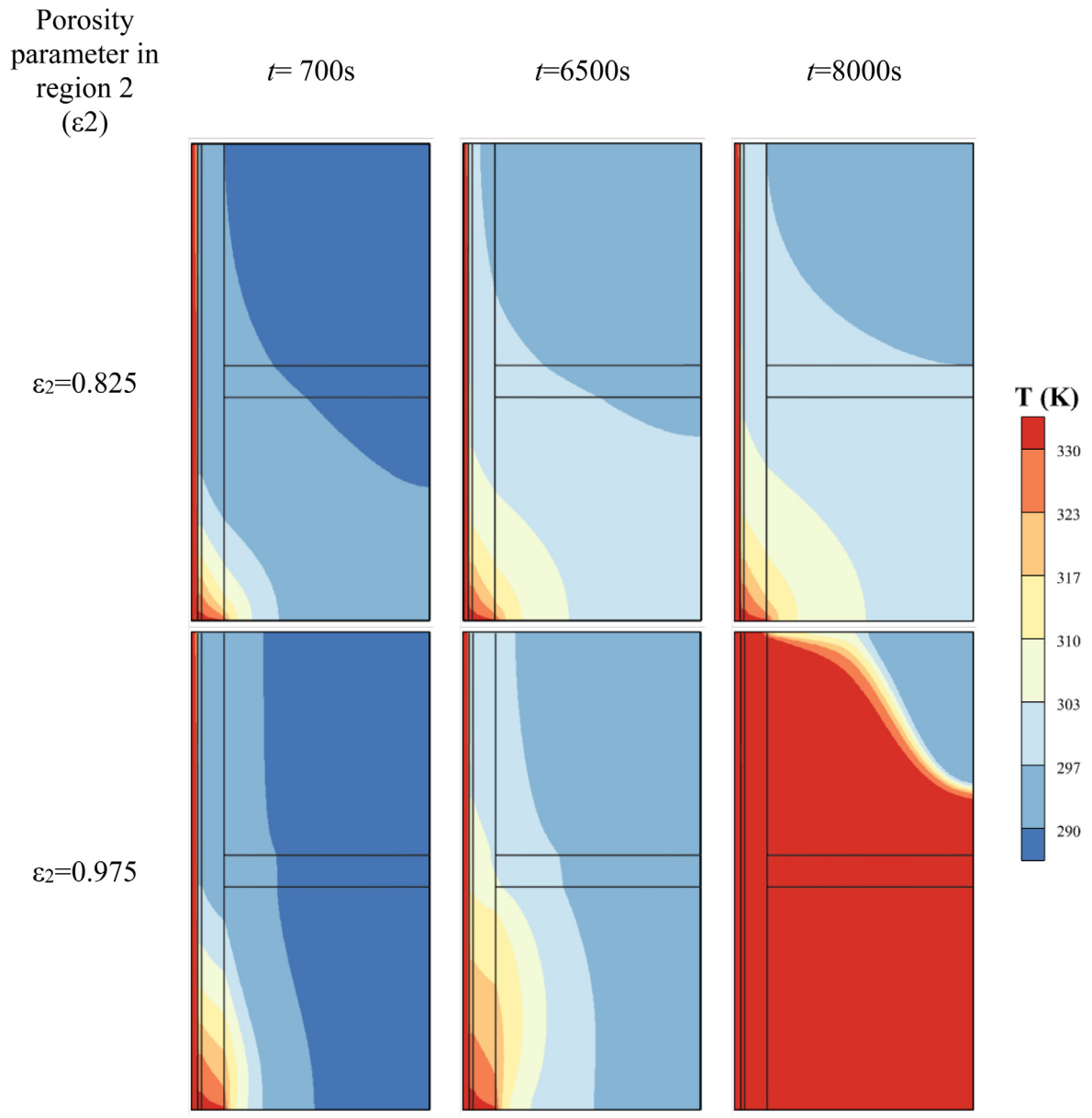

Fig. 12. Effect of porosity parameter in the region 2 (ε_2) on the contours of isotherm; ε_2=0.825 (top row) and ε_2=0.975 (bottom row).

The initial condition for the PCM domain can be expressed as the following:

$$u|_{PCM} = w|_{PCM} = 0,\ P|_{PCM} = 0,\ T|_{PCM} = T_{initial} \tag{23}$$

2.4. Characteristics parameters

The total stored energy (ES) in the annuli is computed as

$$ES(t) = \text{Sensibleenergy} + \text{Latentheatenergy} \tag{24}$$

where $\text{Latentheatenergy} = \int_V \varepsilon \rho_{LPP} h_{LPP} dV$. Besides, the melting volume fraction (MVF) is computed as

$$MVF(t) = \frac{\int_V \varepsilon \omega(T) dV}{\int_V \varepsilon dV} \tag{25}$$

where $dV=2\pi r dr$ is the volume element of the enclosure.

The outlet flow rate was introduced as

$$Q_{out} = \int_A w\, dA$$

where $dA=rdr$ is the surface element of the outlet. The outlet average temperature difference ($\Delta\bar{T}_{out}$) is introduced as

$$\Delta\bar{T}_{out}(t) = \frac{\int_A \frac{w}{\bar{w}}(T_h - T) dA}{\int_A dA} \tag{26}$$

where $\bar{w} = \int_A w\, dA / \int_A dA$. The geometrical details of the enclosure are as follows: R_p= 6.35 mm (1/4 in), Lb=0.2032 m (8 in), Hb=0.4064 m (16 in), $t_{mf} = 3R_p$, $H_{mf} = Hb/15$, t_p= 3.175 mm (1/8 in).

3. Numerical method, mesh study, and verification

The finite element method (FEM) was employed to solve the governing equations and the boundary conditions.

3.1. Numerical method

A weak form of governing equations was integrated over mesh elements using the FEM to obtain residual equations using a

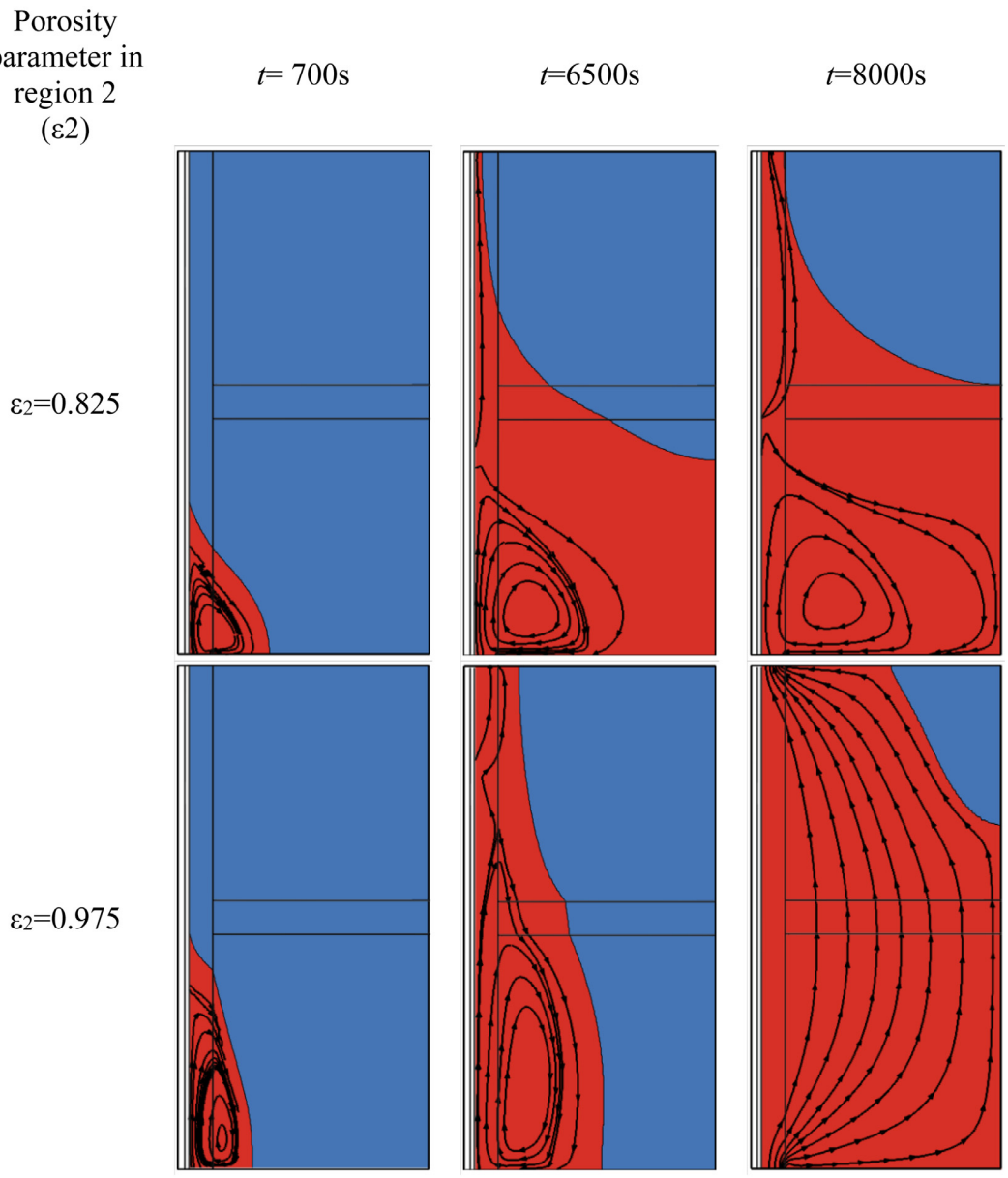

Fig. 13. Effect of porosity parameter in the region 2 (ε_2) on the streamlines; ε_2=0.825 (top row) and ε_2=0.975 (bottom row).

second-order formula. Then the PARDISO (PARallel DIrect Solver) solver [53–55] was employed to solve the equations. The Newton method with a damping factor of 0.8 was invoked to solve the coupled form of the equations. A first-second order backward differential formula [56] was employed to select the computational time steps and control the solution accuracy smaller than 10^{-4}. The computations were suppressed when the melting volume fraction reached a value larger than 0.999.

3.2. Mesh study

The mesh study was performed to check the impact of the mesh size on the accuracy of the computations. A structured mesh was used for the discretization of the computational domain. The computations were repeated for four different meshes. The mesh size was controlled using an integer variable (N) where N=2, 3, 4, and 5. The details of the utilized mesh are as follows: the inlet and outlet of the HTF region ($5N$ mesh points) with a non-uniform stretching element ratio of 0.05. So, the mesh next to the HTF tube is denser than the central regions. $101N$ mesh points for the height of the system, where $7N$ points were used for meshing the extended metal foam region. The $2N$ and $4N$ mesh points were used for the inlet/outlet and wall thickness, respectively. Moreover, $35N$ points were used for the rest of the horizontal walls of the annuli space. $6N$ mesh points were also used for the metal foam layer over the HTF tube. A view of the utilized mesh for N=3 is illustrated in Fig. 3. The computations were executed for a case with ε_1=0.9, ε_2=0.975, $t_{\text{porous}}=3R_p$, P_{in}=1500 Pa, U_0=0.1m/s, and NL=0 and the results are shown in Fig. 4. As seen, the computed results for the case of low-resolution mesh (N=2) are slightly different from other cases (N>2). However, there is no apparent difference between cases N=3, 4, and 5. Thus, increasing the mesh size over N=3 does not add notable computational accuracy to the results. Hence, in order to save computational time and resources, the mesh size of N=3 was adopted for the computations. The resulting mesh is made of 43,200 quad elements.

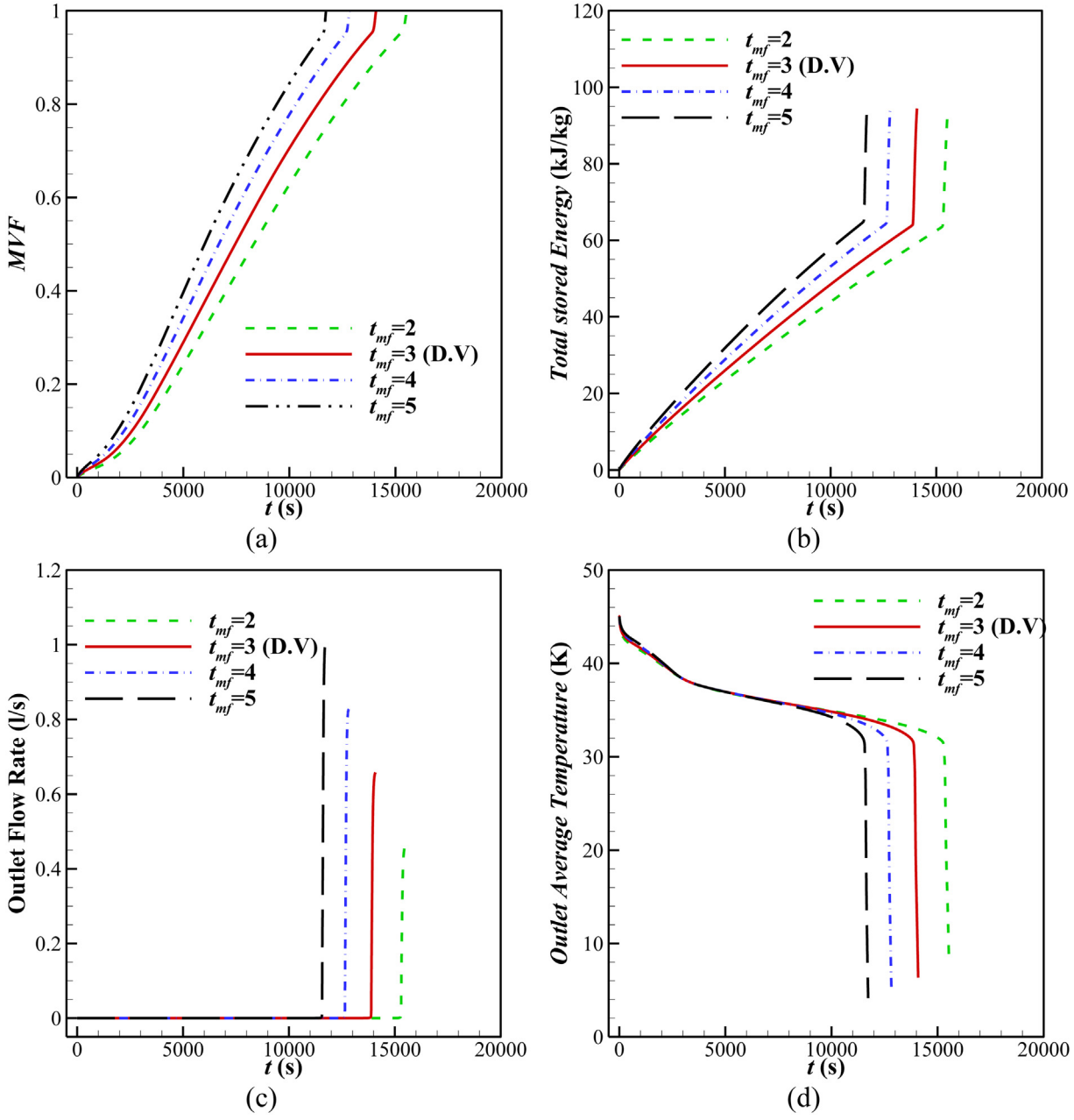

Fig. 14. Effect of thickness of porous region (t_{mf}) on the (a) melting volume fraction, (b) total stored energy, (c) outlet flow rate, and (d) outlet average temperature.

3.3. Code verification

The code precision and model were examined by making a comparison with the experimental data of Kamkari et al. [57]. In [57], the melting of lauric acid PCM was investigated in a 120 × 50 mm enclosure. The enclosure surfaces were well insulated except for its left vertical wall, which was exposed to a heat source. The same model was simulated here, and the *MVF* is compared to the literature's theoretical [58] and experimental [57] data in Fig. 5. As seen, the simulated and examined data well agree and confirm the accuracy of the computations and the model. Moreover, the simulation results of the present model and code were compared with the results of [50,51] during a melting process of a PCM in an enclosure filled with metal foam. In all cases, an acceptable agreement was observed. Here, the details were omitted for the sake of brevity.

4. Results and discussion

The impact of the porosity of the metal foam layer over the HTF tube (ε_1), the porosity of the extended metal foam region (ε_2), the thickness ratio of the metal foam over the HTF tube (t_{mf}/R_p), and the mounting height of the extended metal foam layer (NL) were investigated on the rate of the thermal energy storage. The thickness of the extended metal foam layer was adjusted with the condition that the total volume of the metal foam remains constant.

The Taguchi method is an optimization approach for improving the quality of products. It explores an orthogonal space of control variables to efficiently search the variable space with minimal cost and find an optimum combination of control parameters. Since the phase change heat transfer simulations are computationally expensive, the Taguchi method seems a good approach for minimizing the charging time. The Taguchi method has been suc-

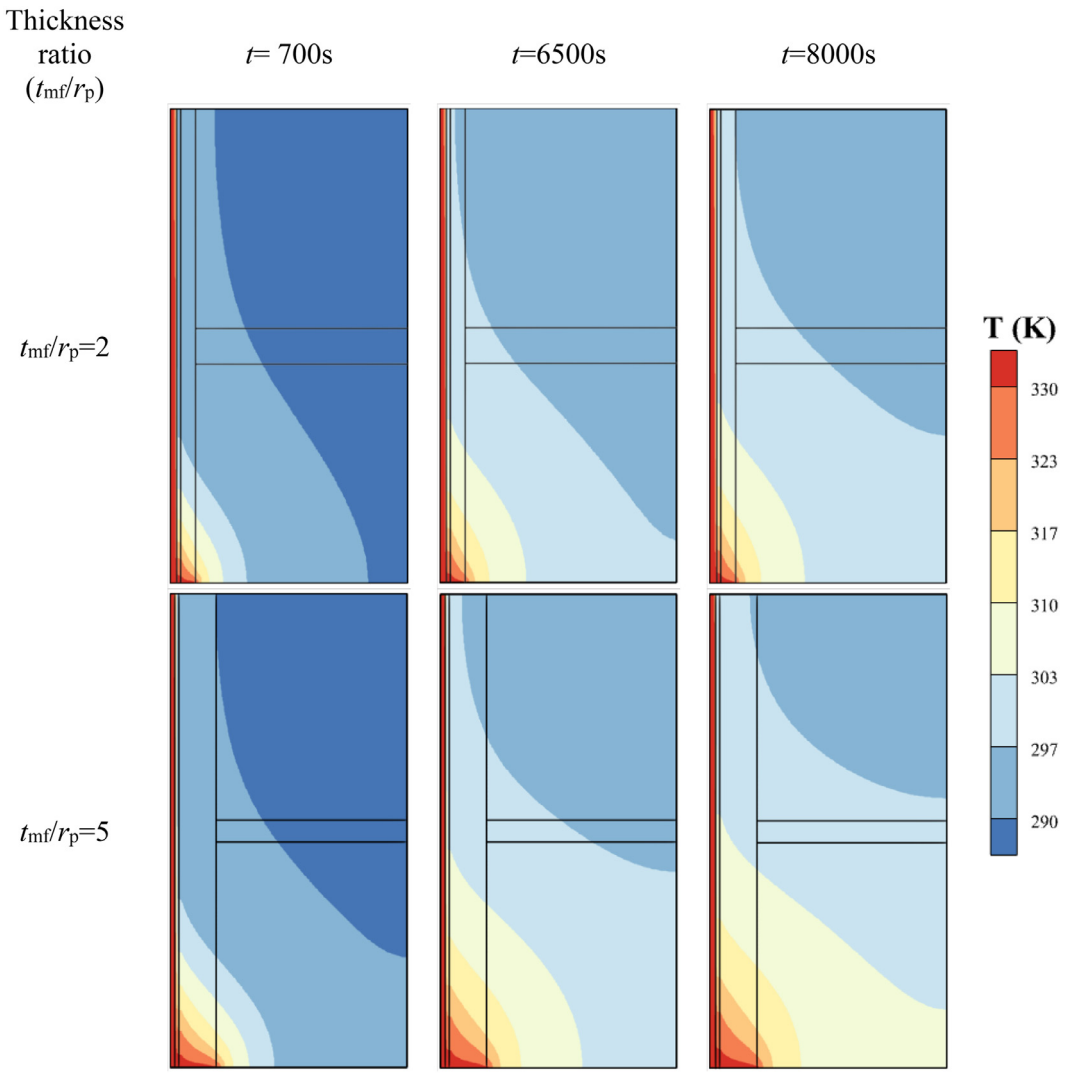

Fig. 15. Effect of thickness ratio (t_{mf}/r_p) on the contours of isotherm; t_{mf}/r_p=2 (top row) and t_{mf}/r_p=5 (bottom row).

cessfully employed in some recent publications related to LHTES, such as [59,60]. Here, the Taguchi method has been used to find the optimum values of porosities (ε_1 and ε_2), the metal foam ratio, and the height ratio of the fin to minimize the melting time.

The design variable and the range and selected level of the variables are summarized in Table 2. Then, following the Taguchi method, an orthogonal table L16 was selected to explore the design space, as reported in Table 3. The time until the melting reaches 95% (MVF=0.95) was adopted as the design goal. The aim is to minimize the melting time.

Moreover, the charging power was computed as $P= ES/t$ where P shows the charging power, ES is the energy storage (Eq. (24)) and t is the charging time. The corresponding charging time, stored energy, and charging power are reported in Table 4. Using the reported data of Table 3, a variable called signal-to-noise ratio (S/N) was obtained using the "the higher, the better" approach of the Taguchi method, as explained in [61–63]. The higher the S/N, the better the obtained design.

Fig. 6 shows the computed S/N values with respect to the charging time. The levels with the highest S/N should be selected as the optimum design. Thus, based on Fig. 6, the optimum design variables are ε_1=0.975, ε_2=0.975, t_{mf}/R_p=5, and NL=-4. The simulations were executed for this design case, and the minimum charging time of 2376s was computed, which confirms that the Taguchi method correctly estimated the optimum design case.

This section investigates the impact of design variables on some of the characteristic parameters. A design case with ε_1=0.875, ε_2=0.875, t_{mf}/R_p=3, and NL=0 is adopted as the reference case, and the design variables were changed around this case. The simulated cases in this section are summarized in Table 4.

Fig. 7 depicts the isotherms and streamlines for the reference (default case) with ε_1=0.875, ε_2=0.875, t_{mf}/R_p=3, and NL=0. As seen, the HTF tube is depicted by a red color since hot water with a fair velocity flows through the tube, and the PCM could only absorb a small amount of HTF heat due to limited heat transfer between the HTF and PCM inside the enclosure. The limited heat transfer is due to the small tube surface and limited convective heat transfer coefficient on the HTF side (laminar flow) and the PCM side (natural convection flow). Initially, t=700 s, only at the bottom portion of the enclosure next to the heated inlet port and HTF tube are heated, and the rest of the enclosure is at a super cold temperature. The streamlines also show small natural convection effects at the bottom. At this stage, there is no film of liquid PCM between the inlet and outlet of the enclosure, and there is no forced convection heat transfer. After a while, t=6500 s, a film of liquid PCM forms over the tube, and a liquid passage between the inlet and outlet of the enclosure forms. The formation of the liquid

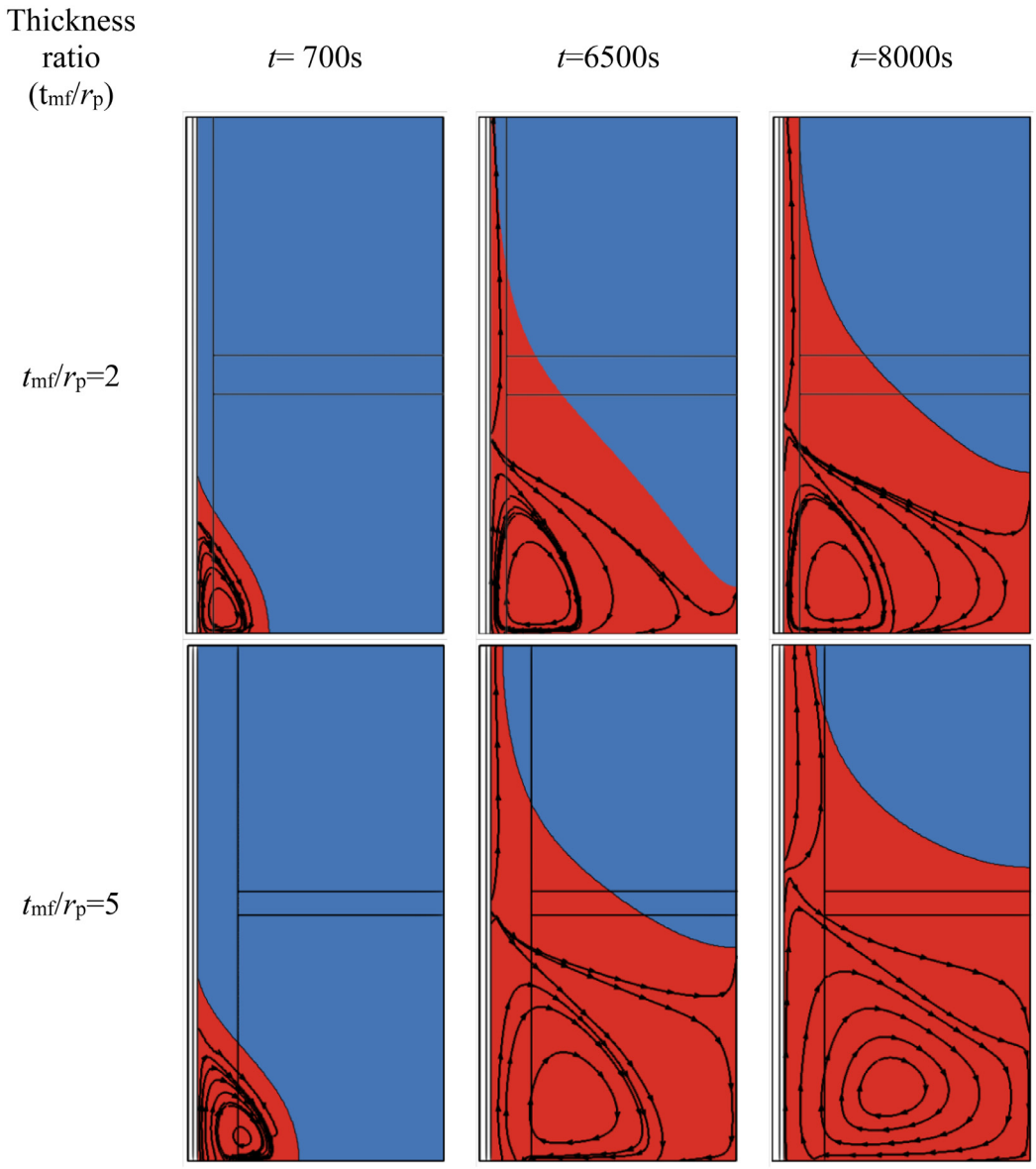

Fig. 16. Effect of thickness ratio (t_{mf}/r_p) on the streamlines; t_{mf}/r_p=2 (top row) and t_{mf}/r_p=5 (bottom row).

film is mainly due to the heat transfer between HTF fluid inside the tube and the PCM around the tube. The streamlines also confirm the formation of a small passage between the inlet and outlet ports of the enclosure. As time passes (t=8000 s), the melting front moves upward, and the forced convection strength increases. Fig. 8, depicts the impact of ε_1 on the characteristic parameters. Moreover, Figs. 9 and 10 depict the impact of ε_1 on the isotherms and streamlines for two porosity values of ε_1=0.825 and ε_1=0.975.

Fig. 8(a) plots the MVF for various values of ε_1. This figure interestingly shows that for the case of ε_1=0.975, the full melting takes place quickly, while for other cases, it takes much longer. This is an unexpected outcome since the increase of the porosity reduces the amount of metal foam and consequently reduces the effective thermal conductivity. However, attention to the physical mechanism of heat transfer in this study confirms that the stream of the liquid PCM and the creation of a liquid passage PCM between the inlet and outlet could lead to the commencing of the foced/mixed convection heat transfer mechanism in the enclosure. When ε_1 is small, the effective thermal conductivity is high. The absorbed heat from the HTF tube propagates in the supper cold PCM quickly and increases the temperature of the PCM by conduction mechanism. However, when ε_1 increases, the effective thermal conductivity of composite PCM reduces. The absorbed heat remains a small later over the tube and melts a small film of PCM around the tube. Thus, for a design with large ε_1, the liquid film's formation accelerates, and the full melting takes place quickly.

The curves of total stored energy (Fig. 8(b)) also follow the same characteristics as MVF. This is because latent heat is the dominant mechanism of thermal energy storage, and the sharp increase of MVF at 800 s could also be expected in Fig. 8(b). Moreover, as seen in Fig. 8(c), the outlet flow rate is initially zero since there is no liquid film passage between the inlet and outlet. However, as soon as a liquid film passage forms, the outlet flow rate increases sharply. Initially, the average outlet temperature difference is high since there is no flow stream between the heated inlet liquid PCM and the outlet at the initial cold temperature. However, due to the heat transfer between the tube and HTF, the temperature next to the outlet increases, and the temperature difference drops. After forming the liquid film, the temperature difference reduces since a high amount of the heated liquid PCM enters the

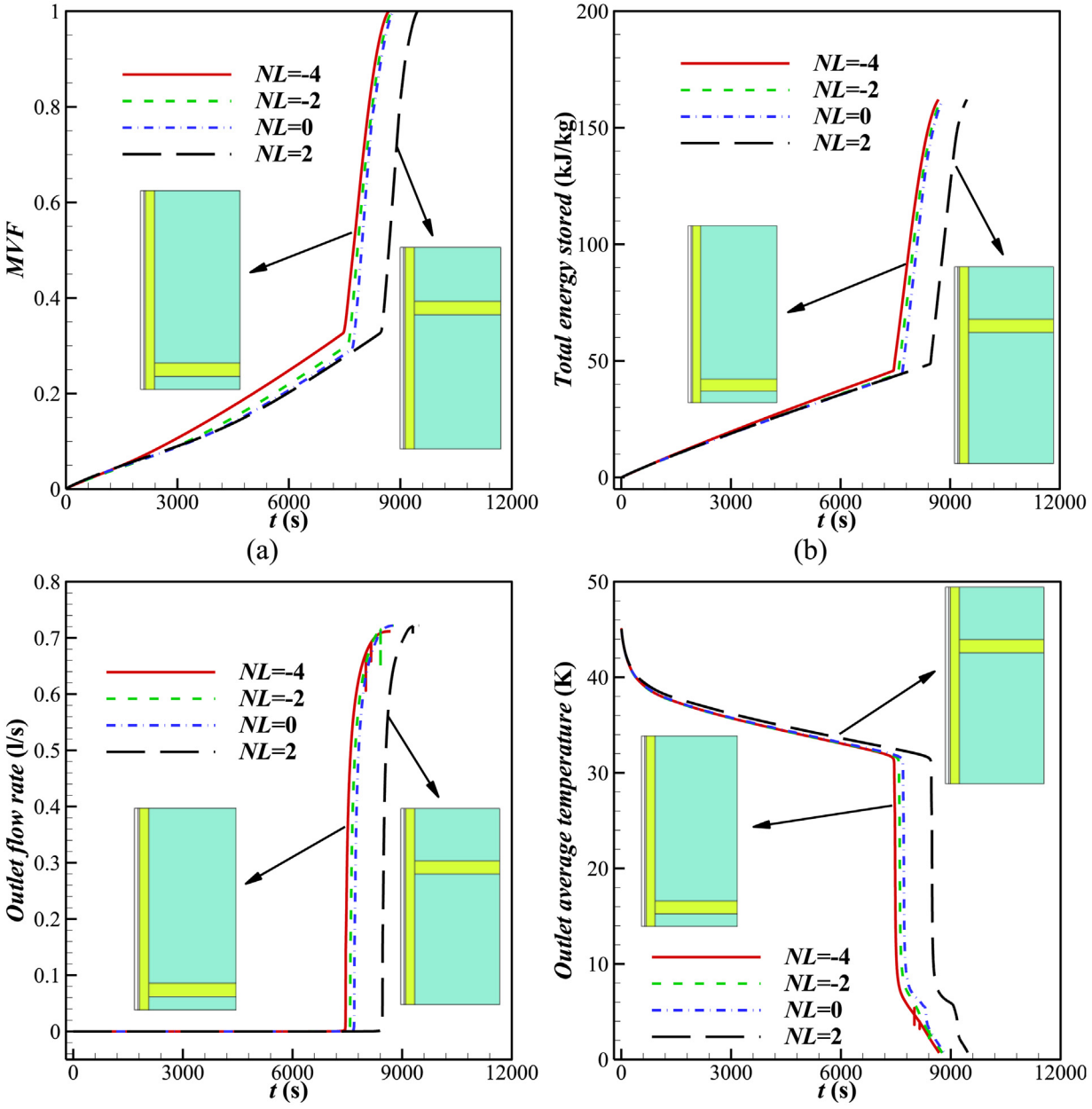

Fig. 17. Effect of the height ratio of fin on the (a) melting volume fraction, (b) total stored energy, (c) outlet flow rate, and (d) outlet average temperature.

enclosure, loses a small amount of its heat to the PCM in the enclosure, and then leaves the enclosure with a small temperature difference with respect to the inlet. These conclusions agree with the observations of Figs. 9 and 10. The effective thermal conductivity of the metal foam and PCM is the most dominant parameter for the formation of liquid film over HTF and charging time. However, permeability can also play a role when the dynamic melting commences. The permeability of foam layers impacts the flow rate and the convection heat transfer.

Fig. 11 depicts the impact of ε_2 on the characteristic parameters and Figs. 12 and 13 illustrate the corresponding isotherms and streamlines for two cases of ε_2= 0.825 and ε_2=0.975 while other parameters are fixed at reference values. These figures show an extended metal foam layer with a high porosity resulting in a quick melting process. An extended surface with high porosity delays liquid film formation over the HTF tube since it helps with a better conduction heat transfer and diffusion of absorbed heat from the HTF tube into the super cold regions of the enclosure. Thus, as seen in Fig. 13, the streamlines between the inlet of the enclosure and its outlet are well developed in the case of ε_2=0.975 and t=8000 s, while for the same time snap, but for ε_2=0.825, the liquid film is about to be established.

Moreover, a larger value of ε_2 leads to a better porous permeability which, as a result, increases the outlet flow rate (as seen in Fig. 11(c)). The amount of final stored energy also rises with the increase of ε_2 since the number of void spaces increases, and consequently, more PCM can be embedded in the enclosure. The effective thermal conductivity of foam with high porosity is small, and thus, the local temperature of PCM next to HTF can increase more quickly, which allows a fast formation of dynamic melting. The lowest average outlet temperature difference can be seen for the case with ε_2=0.975, which is due to the highest flow rate for this case.

Figs. 14–16 depict the impact of the metal foam ratio on the characteristic parameter, isotherms, and streamlines. These figures show the foam ratio could slightly change the thermal charging

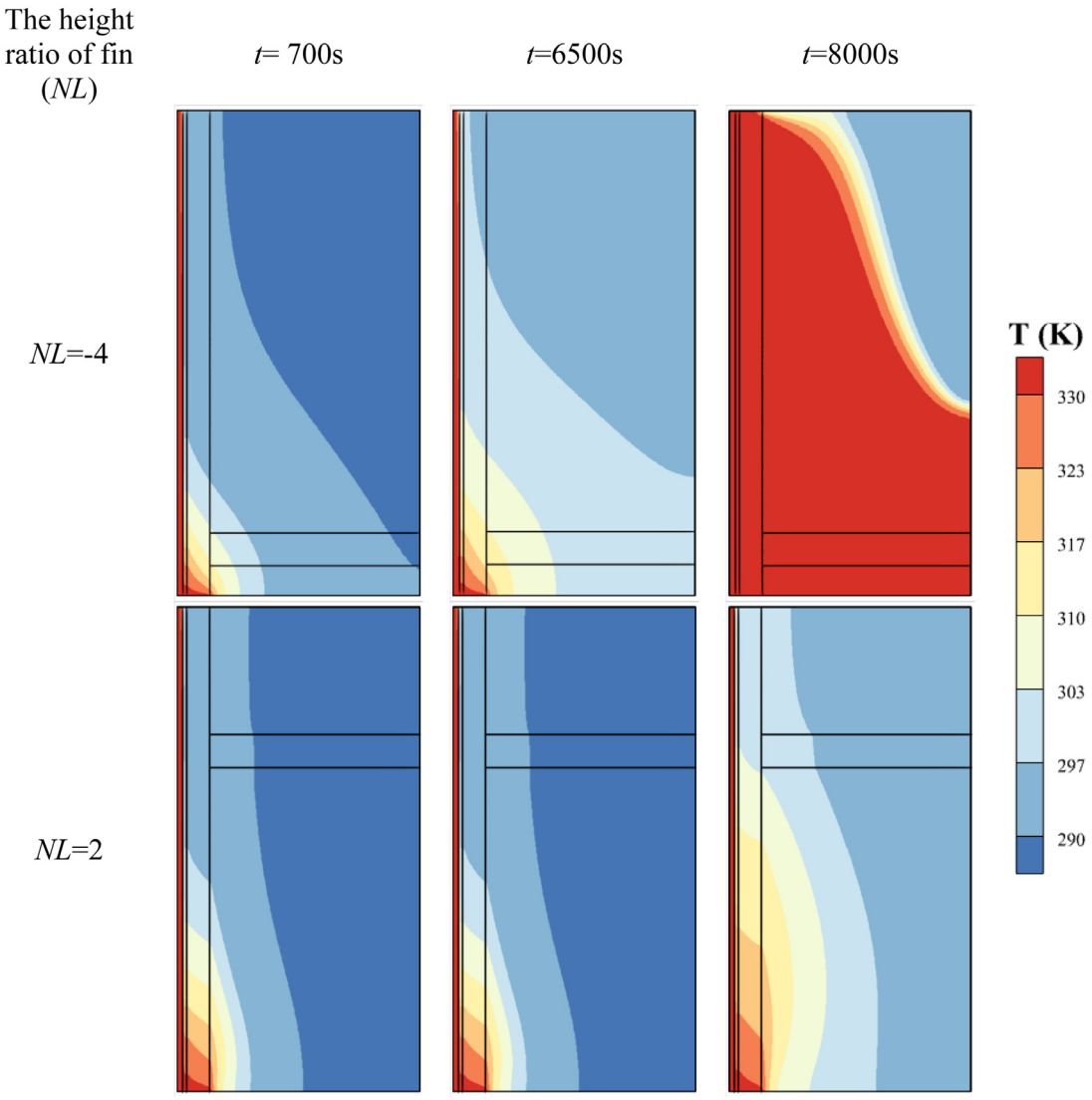

Fig. 18. Effect of height ratio of fin (*NL*) on the contours of isotherm; *NL*=-4 (top row) and *NL*=2 (bottom row).

behavior of the unit. A larger value of foam ratio means a thicker foam layer over the HTF tube and a thinner extended foam layer. As seen, a thick foam layer over the tube could better melt the PCM inside the enclosure compared to a thin one.

Moreover, the amount of final stored energy is not a function of the foam ratio since the total amount of foam is fixed, and thus the total amount of the PCM embedded in the foam cannot be changed. From Fig. 14, it can be seen the liquid film can be formed slightly faster for a large value of foam ratio. The location of film formation can be estimated in Fig. 14 from the sharp rise of the characteristics parameters. When the extended surface is narrow, it cannot properly channel the heat from the HTF tube into the supper cold PCM by conduction mechanism and prevent the formation of early liquid film over the HTF tube. Moreover, a large foam ratio leads to a higher outlet flow rate since only a thin layer of extended foam resists the fluid motion. Consequently, a small temperature difference could be observed at final times when the foam ratio is high due to the corresponding large outlet flow rate. As seen in Fig. 16, the streamlines are well developed in the enclosure at t=8000 s when the foam ratio is five compared to that of foam ratio equal to two.

Figs. 17–19 depict the impact of extended foam layer location (*NL*) on the characteristic parameters, isotherms, and streamlines. As seen, there is not much difference between the mounting location of the extended foam layer when the foam is mounted in the middle or toward the bottom. However, mounting the extended layer toward the top delays the melting process. Attention to Figs. 17–19 shows that placing the extended foam layer at the top delays liquid film formation over the HTF tube. Indeed, the liquid film formation starts from the bottom, where the heat transfer between the HTF flow and the tube surface (PCM region) is the strongest. As the HTF moves upward, its heat transfer coefficient and temperature drop.

As discussed earlier, the extended foam layer contributes to the conduction heat transfer and channels some of the HTF heat into the super cold PCM regions, thus delaying forming the liquid film. Placing the extended layer at the top delays forming the liquid film, which was already weak due to the low heat transfer rate between HTF and PCM. Figs. 18 and 19 also show that the convection heat transfer between the intel and outlet ports of the enclosure are well established for *NL*=-4 and t=8000 s, while for the case *NL*=2 and t=8000 s, the liquid film is just about to be developed. The amount of stored energy follows the MVF pattern, and the total stored energy is fixed since the amount of foam layer and PCM are fixed. The ultimate outlet flow rate is also fixed for various values of *NL* since it induces a flow resistance against the forced con-

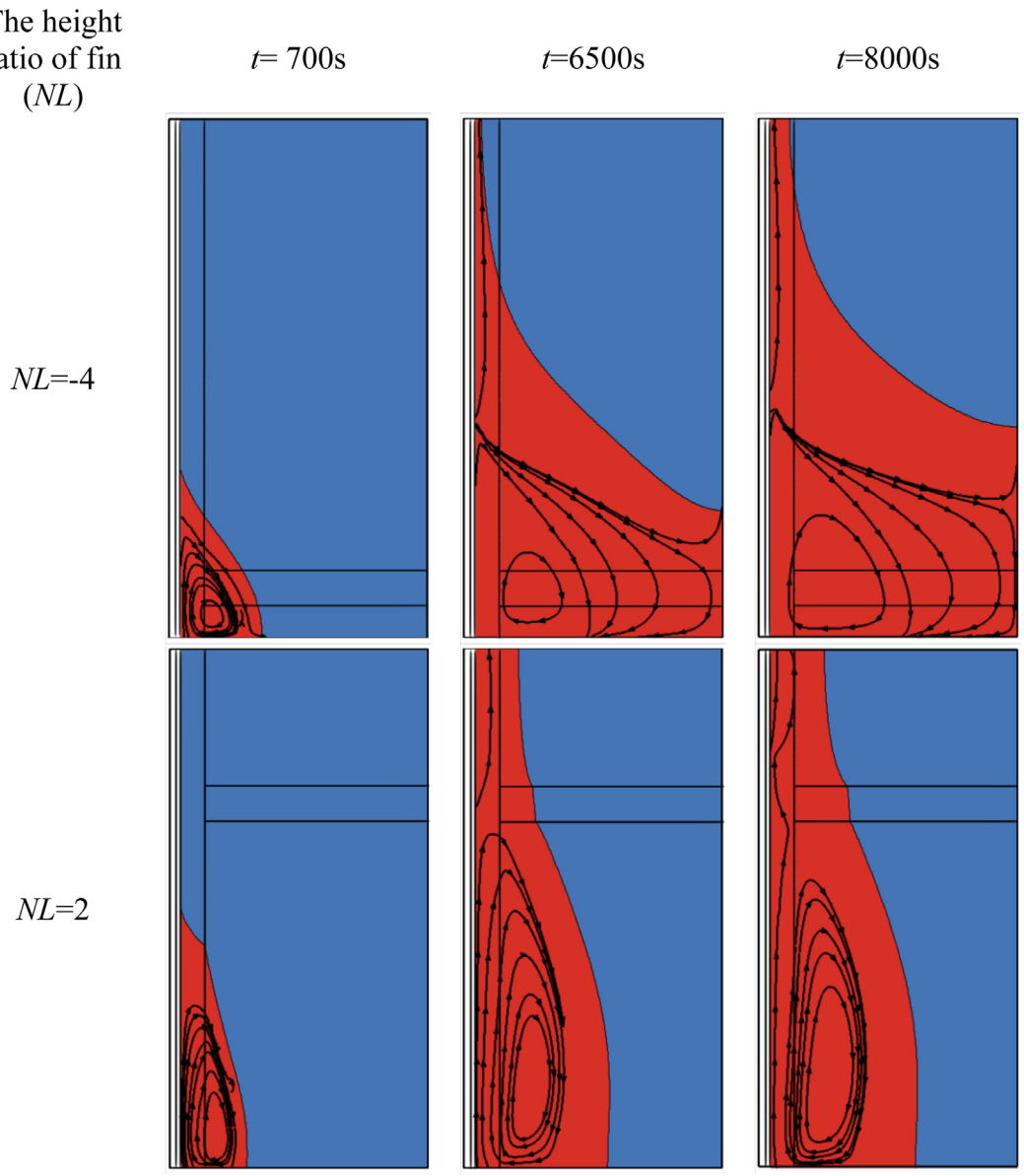

Fig. 19. Effect of height ratio of fin (*NL*) on the streamlines; *NL*=-4 (top row) and *NL*=2 (bottom row).

vection liquid PCM almost regardless of its position. Finally, since the ultimate outlet flow rates are similar, the ultimate outlet average temperature differences are also similar.

In conventional closed storage systems, heat transfer occurs through the enclosure surfaces. Thus, there is a heat transfer limitation at the enclosure surface since the surface of the enclosure can reach the HTF temperature as the convection heat transfer tends to infinity. Then, the internal thermal resistance of the enclosure acts as a barrier to fast charging of the storage unit due to the limited thermal conductivity of the PCM. In contrast, the present design profits from a strong convective heat transfer mechanism, which is supported by a pressurized heat transfer flow of liquid PCM moving through the enclosure. A fast charging mechanism makes the design appropriate for energy transport from power plants to commercial renewable energy sites. The liquid PCM can be circulated in a thermodynamic cycle and recover waste heat. Then, the heated liquid PCM enters the storage unit to charge the unit quickly. The advantage of the present design is attributed to the direct contact nature of liquid PCM with the solid PCM in the storage unit.

5. Conclusion

The melting heat transfer and thermal energy storage of a new design of thermal energy storage were addressed in the present study. In the proposed design, a pressurized stream of heated liquid PCM could enter the enclosure and accelerate the heat transfer and the thermal charging process. An HTF tube was placed in the center of the thermal energy storage unit to assist the creation of a thin film of liquid PCM and open a passage between the enclosure's inlet and outlet ports, allowing heated liquid PCM to enter and leave the enclosure. Two layers of metal foam with different porosities were employed in the enclosure to support the heat transfer around the HTF tube and inside the enclosure. The finite element method was employed to solve the governing equations in the HTF tube, tube wall, and PCM enclosure. The impact of foam layer porosities, foam layer ratio, and location of extended foam layer were studied on the MVF, stored thermal energy, outlet flow rate, and average outlet temperature. The isotherms and streamlines were also plotted to express the physical behavior of the system.

The results showed that using a metal foam with high porosity not only increases the capacity of the thermal energy storage unit but also accelerates the charging process. This observation is against the conventional literature data regarding the melting heat transfer enhanced with metal foams in closed enclosures. In the sealed enclosures, the increase of porosity reduces the effective thermal conductivity; thus, the melting rate is expected to be reduced. However, in the present design, in which there is a mixed convection flow, a metal foam layer with high porosity results in an effective low composite thermal conductivity over the HTF tube and accelerates the formation of a liquid PCM film over the HTF tube. Moreover, a high porosity extended foam layer reduces the overall flow resistance for the stream of heated liquid PCM and also accelerates the formation of the liquid film passage between the inlet and outlet ports of the enclosure, which consequently reduces the thermal charging time of the system.

Increasing the foam ratio (increasing the metal foam layer thickness over the HTF tube) reduces the thermal charging time by accelerating the formation of thin PCM liquid film and reducing the resistance to the heated liquid PCM stream.

The location of the extended foam influences the melting time insignificantly except when the foam is mounted at the top of the enclosure, which increases the charging time by delaying the liquid film formation. Thus, it could be concluded that using an extended foam in the enclosure is not much beneficial.

The results showed that the formation of the initial liquid film is the most significant parameter which could control the charging time. Thus, charging enclosures with a minimum charge (not supper cold PCM) or using an electrical element instead of the HTF tube maybe accelerate the charging process further, which could be the subject of future research studies. Moreover, since the metal foam can impact the results, the thickness of the foam layers and their pore density can also impact the results, which could be the subject of future studies.

Declaration of Competing Interest

The authors clarify that there is no conflict of interest for report.

CRediT authorship contribution statement

Mehdi Ghalambaz: Conceptualization, Methodology, Software, Validation, Formal analysis, Data curation. **Mutabe Aljaghtham:** Visualization, Writing – original draft, Investigation, Formal analysis, Data curation. **Ali J. Chamkha:** Visualization, Writing – original draft, Investigation, Formal analysis, Data curation. **Abdelkader Abdullah:** Methodology, Software, Formal analysis, Data curation. **Umar Alqsair:** Methodology, Software, Formal analysis, Data curation. **Mohammad Ghalambaz:** Investigation, Writing – review & editing, Supervision.

Data availability

No data was used for the research described in the article.

Acknowledgments

The authors extend their appreciation to the Deputyship for Research & Innovation, Ministry of Education in Saudi Arabia for funding this research work through the project number (IF-PSAU-2021/01/18928).

References

[1] W. Liu, Y. Bie, T. Xu, A. Cichon, G. Królczyk, Z. Li, Heat transfer enhancement of latent heat thermal energy storage in solar heating system: a state-of-the-art review, J. Energy Storage 46 (2022) 103727.
[2] J. Gasia, L. Miró, L.F. Cabeza, Review on system and materials requirements for high temperature thermal energy storage, Part 1 Gen. Requir. Renew. Sustain. Energy Rev. 75 (2017) 1320–1338.
[3] B. Ma, D. Shin, D. Banerjee, One-step synthesis of molten salt nanofluid for thermal energy storage application – a comprehensive analysis on thermophysical property, corrosion behavior, and economic benefit, J. Energy Storage 35 (2021) 102278.
[4] Z.A. Qureshi, H.M. Ali, S. Khushnood, Recent advances on thermal conductivity enhancement of phase change materials for energy storage system: a review, Int. J. Heat Mass Transf. 127 (2018) 838–856.
[5] A.K. Pandey, M.S. Hossain, V.V. Tyagi, N.A. Rahim, J.A.L. Selvaraj, A. Sari, Novel approaches and recent developments on potential applications of phase change materials in solar energy, Renew. Sustain. Energy Rev. 82 (2018) 281–323.
[6] Y.B. Tao, Y.L. He, A review of phase change material and performance enhancement method for latent heat storage system, Renew. Sustain. Energy Rev. 93 (2018) 245–259.
[7] X. Yang, P. Wei, X. Wang, Y.L. He, Gradient design of pore parameters on the melting process in a thermal energy storage unit filled with open-cell metal foam, Appl. Energy 268 (2020) 115019.
[8] X. Yang, X. Wang, Z. Liu, Z. Guo, L. Jin, C. Yang, Influence of aspect ratios for a tilted cavity on the melting heat transfer of phase change materials embedded in metal foam, Int. Commun. Heat Mass Transf. 122 (2021) 105127.
[9] H. Masoumi, R.H. Khoshkhoo, Investigation of melting of nanoparticle-enhanced phase change materials (NePCMs) in a shell-and-tube heat exchanger with longitudinal fins, Heat Mass Transf. 57 (4) (2020) 681–701.
[10] X.K. Yu, Y.B. Tao, Y. He, Z.C. Lv, Preparation and performance characterization of metal foam/paraffin/single-walled carbon nanotube composite phase change material, Int. J. Heat Mass Transf. 191 (2022) 122825.
[11] H. Masoumi, R.H. Khoshkhoo, S.M. Mirfendereski, Experimental and numerical investigation of melting/solidification of nano-enhanced phase change materials in shell & tube thermal energy storage systems, J. Energy Storage 47 (2022) 103561.
[12] A.I. Fernández, C. Barreneche, M. Belusko, M. Segarra, F. Bruno, L.F. Cabeza, Considerations for the use of metal alloys as phase change materials for high temperature applications, Sol. Energy Mater. Sol. Cells 171 (2017) 275–281.
[13] I. Sarbu, A. Dorca, Review on heat transfer analysis in thermal energy storage using latent heat storage systems and phase change materials, Int. J. Energy Res. 43 (1) (2018) 29–64.
[14] N.I. Ibrahim, F.A. Al-Sulaiman, S. Rahman, B.S. Yilbas, A.Z. Sahin, Heat transfer enhancement of phase change materials for thermal energy storage applications: A critical review, Renew. Sustain. Energy Rev. 74 (2017) 26–50.
[15] M. Esapour, A. Hamzehnezhad, A.A.R. Darzi, M. Jourabian, Melting and solidification of PCM embedded in porous metal foam in horizontal multi-tube heat storage system, Energy Convers. Manag. 171 (2018) 398–410.
[16] X. Yang, J. Yu, Z. Guo, L. Jin, Y.L. He, Role of porous metal foam on the heat transfer enhancement for a thermal energy storage tube, Appl. Energy 239 (2019) 142–156.
[17] H.I. Mohammed, P. Talebizadehsardari, J.M. Mahdi, A. Arshad, A. Sciacovelli, D. Giddings, Improved melting of latent heat storage via porous medium and uniform Joule heat generation, J. Energy Storage 31 (2020) 101747.
[18] P.T. Sardari, H.I. Mohammed, D. Giddings, M. Gillott, D. Grant, Numerical study of a multiple-segment metal foam-PCM latent heat storage unit: effect of porosity, pore density and location of heat source, Energy 189 (2019) 116108.
[19] J.M. Mahdi, H.I. Mohammed, E.T. Hashim, P. Talebizadehsardari, E.C. Nsofor, Solidification enhancement with multiple PCMs, cascaded metal foam and nanoparticles in the shell-and-tube energy storage system, Appl. Energy 257 (2020) 113993.
[20] Z. Wang, J. Wu, D. Lei, H. Liu, J. Li, Z. Wu, Experimental study on latent thermal energy storage system with gradient porosity copper foam for mid-temperature solar energy application, Appl. Energy 261 (2020) 114472.
[21] S.N.J. Ercan Mehmet DEDEThermal Management Systems Including Multiple Phase Changing Materials and Vehicles Including the Same, Toyota Motor Engineering & Manufacturing North America, Inc., Plano, TX (US), United States, 2018.
[22] V. Joshi, M.K. Rathod, Thermal performance augmentation of metal foam infused phase change material using a partial filling strategy: An evaluation for fill height ratio and porosity, Appl. Energy 253 (2019) 113621.
[23] Z.Q. Zhu, Y.K. Huang, N. Hu, Y. Zeng, L.W. Fan, Transient performance of a PCM-based heat sink with a partially filled metal foam: Effects of the filling height ratio, Appl. Therm. Eng. 128 (2018) 966–972.
[24] T.X. Li, D.L. Wu, F. He, R.Z. Wang, Experimental investigation on copper foam/hydrated salt composite phase change material for thermal energy storage, Int. J. Heat Mass Transf. 115 (2017) 148–157.
[25] R.S. Ferfera, B. Madani, Thermal characterization of a heat exchanger equipped with a combined material of phase change material and metallic foams, Int. J. Heat Mass Transf. 148 (2020) 119162.
[26] M. Iasiello, M. Mameli, S. Filippeschi, N. Bianco, Metal foam/PCM melting evolution analysis: orientation and morphology effects, Appl. Therm. Eng. 187 (2021) 116572.
[27] K. Lafdi, O. Mesalhy, S. Shaikh, Experimental study on the influence of foam porosity and pore size on the melting of phase change materials, J. Appl. Phys. 102 (8) (2007) 083549.
[28] M. Iasiello, M. Mameli, S. Filippeschi, N. Bianco, Simulations of paraffine melting inside metal foams at different gravity levels with preliminary experimental validation, J. Phys. Conf. Ser. (2020) 012008 IOP Publishing.

[29] A. Ghahremannezhad, H. Xu, M.R. Salimpour, P. Wang, K. Vafai, Thermal performance analysis of phase change materials (PCMs) embedded in gradient porous metal foams, Appl. Therm. Eng. 179 (2020) 115731.
[30] A. NematpourKeshteli, M. Iasiello, G. Langella, N. Bianco, Enhancing PCMs thermal conductivity: a comparison among porous metal foams, nanoparticles and finned surfaces in triplex tube heat exchangers, Appl. Therm. Eng. 212 (2022) 118623.
[31] A. Arshad, M. Jabbal, H. Faraji, P. Talebizadehsardari, M.A. Bashir, Y. Yan, Thermal performance of a phase change material-based heat sink in presence of nanoparticles and metal-foam to enhance cooling performance of electronics, J. Energy Storage 48 (2022) 103882.
[32] N.H.S. Tay, M. Liu, M. Belusko, F. Bruno, Review on transportable phase change material in thermal energy storage systems, Renew. Sustain. Energy Rev. 75 (2017) 264–277.
[33] Y. Kozak, T. Rozenfeld, G. Ziskind, Close-contact melting in vertical annular enclosures with a non-isothermal base: theoretical modeling and application to thermal storage, Int. J. Heat Mass Transf. 72 (2014) 114–127.
[34] J.J. Vadasz, J.P. Meyer, S. Govender, G. Ziskind, Experimental study of vibration effects on heat transfer during solidification of paraffin in a spherical shell, Exp. Heat Transf. 29 (3) (2015) 285–298.
[35] F. Hu, D.-W. Sun, W. Gao, Z. Zhang, X. Zeng, Z. Han, Effects of pre-existing bubbles on ice nucleation and crystallization during ultrasound-assisted freezing of water and sucrose solution, Innov. Food Sci. Emerg. Technol. 20 (2013) 161–166.
[36] V. Zipf, A. Neuhäuser, D. Willert, P. Nitz, S. Gschwander, W. Platzer, High temperature latent heat storage with a screw heat exchanger: design of prototype, Appl. Energy 109 (2013) 462–469.
[37] J. Gasia, D. Groulx, N.H.S. Tay, L.F. Cabeza, Numerical study of dynamic melting enhancement in a latent heat thermal energy storage system, J. Energy Storage 31 (2020) 101664.
[38] N.H.S. Tay, M. Belusko, M. Liu, F. Bruno, Investigation of the effect of dynamic melting in a tube-in-tank PCM system using a CFD model, Appl. Energy 137 (2015) 738–747.
[39] N. Tay, F. Bruno, M. Belusko, Experimental investigation of dynamic melting in a tube-in-tank PCM system, Appl. Energy 104 (2013) 137–148.
[40] J. Gasia, N.S. Tay, M. Belusko, L.F. Cabeza, F. Bruno, Experimental investigation of the effect of dynamic melting in a cylindrical shell-and-tube heat exchanger using water as PCM, Appl. Energy 185 (2017) 136–145.
[41] V. Joshi, M.K. Rathod, Thermal transport augmentation in latent heat thermal energy storage system by partially filled metal foam: a novel configuration, J. Energy Storage 22 (2019) 270–282.
[42] M. Ghalambaz, S. Mehryan, A. Hajjar, M.Y.A. Shdaifat, O. Younis, P. Talebizadehsardari, W. Yaïci, Thermal charging optimization of a Wavy-shaped nano-enhanced thermal storage unit, Molecules 26 (5) (2021) 1496.
[43] M.J. Li, M.J. Li, X.D. Xue, D. Li, Optimization and design criterion of the shell-and-tube thermal energy storage with cascaded PCMs under the constraint of outlet threshold temperature, Renew. Energy 181 (2022) 1371–1385.
[44] M. Ghalambaz, S. Mehryan, M. Mahdavi, O. Younis, M.A. Alim, Evaluation of the melting performance in a conical latent heat thermal unit having variable length fins, Sustainability 13 (5) (2021) 2667.
[45] H. Zuo, M. Wu, K. Zeng, Y. Zhou, J. Kong, Y. Qiu, M. Lin, G. Flamant, Numerical investigation and optimal design of partially filled sectorial metal foam configuration in horizontal latent heat storage unit, Energy 237 (2021) 121640.
[46] D.A. Nield, A. Bejan, Convection in Porous Media, Springer, 2006.
[47] Z. Liu, Y. Yao, H. Wu, Numerical modeling for solid–liquid phase change phenomena in porous media: shell-and-tube type latent heat thermal energy storage, Appl. Energy 112 (2013) 1222–1232.
[48] M. Ghalambaz, A.A. Melaibari, A.J. Chamkha, O. Younis, M. Sheremet, Phase change heat transfer and energy storage in a wavy-tube thermal storage unit filled with a nano-enhanced phase change material and metal foams, J. Energy Storage 54 (2022) 105277.
[49] O. Mesalhy, K. Lafdi, A. Elgafy, K. Bowman, Numerical study for enhancing the thermal conductivity of phase change material (PCM) storage using high thermal conductivity porous matrix, Energy Convers. Manag. 46 (6) (2005) 847–867.
[50] H. Zheng, C. Wang, Q. Liu, Z. Tian, X. Fan, Thermal performance of copper foam/paraffin composite phase change material, Energy Convers. Manag. 157 (2018) 372–381.
[51] M. Al-Jethelah, S. Ebadi, K. Venkateshwar, S.H. Tasnim, S. Mahmud, A. Dutta, Charging nanoparticle enhanced bio-based PCM in open cell metallic foams: an experimental investigation, Appl. Therm. Eng. 148 (2019) 1029–1042.
[52] S.K. Choi, S.O. Kim, T.H. Lee, Dohee-Hahn, Computation of the natural convection of nanofluid in a square cavity with homogeneous and nonhomogeneous models, Numer. Heat Transf. Part A Appl. 65 (4) (2014) 287–301.
[53] O. Schenk, K. Gärtner, Solving unsymmetric sparse systems of linear equations with PARDISO, Futur. Gener. Comput. Syst. 20 (3) (2004) 475–487.
[54] P. Wriggers, Nonlinear Finite Element Methods, Springer Science & Business Media, 2008.
[55] F. Verbosio, A. De Coninck, D. Kourounis, O. Schenk, Enhancing the scalability of selected inversion factorization algorithms in genomic prediction, J. Comput. Sci. 22 (2017) 99–108.
[56] G. Söderlind, L. Wang, Adaptive time-stepping and computational stability, J. Comput. Appl. Math. 185 (2) (2006) 225–243.
[57] B. Kamkari, H. Shokouhmand, F. Bruno, Experimental investigation of the effect of inclination angle on convection-driven melting of phase change material in a rectangular enclosure, Int. J. Heat Mass Transf. 72 (2014) 186–200.
[58] B. Kamkari, H.J. Amlashi, Numerical simulation and experimental verification of constrained melting of phase change material in inclined rectangular enclosures, Int. Commun. Heat Mass Transf. 88 (2017) 211–219.
[59] M. Ghalambaz, H.I. Mohammed, J.M. Mahdi, A.H. Eisapour, O. Younis, A. Ghosh, P. Talebizadehsardari, W. Yaïci, Intensifying the charging response of a phase-change material with twisted fin arrays in a shell-and-tube storage system, Energies 14 (6) (2021) 1619.
[60] M. Ghalambaz, A.H. Eisapour, H.I. Mohammed, M.S. Islam, O. Younis, P.T. Sardari, W. Yaïci, Impact of tube bundle placement on the thermal charging of a latent heat storage unit, Energies 14 (5) (2021) 1289.
[61] M.H. Wang, M.L. Huang, Z.Y. Zhan, C.J. Huang, Application of the extension Taguchi method to optimal capability planning of a stand-alone power system, Energies 9 (3) (2016) 174.
[62] X. Sun, Y. Mo, J. Li, Y. Chu, L. Liu, S. Liao, Study on the energy charging process of a plate-type latent heat thermal energy storage unit and optimization using Taguchi method, Appl. Therm. Eng. 164 (2020) 114528.
[63] X. Liu, Y. Zhou, C.Q. Li, Y. Lin, W. Yang, G. Zhang, Optimization of a new phase change material integrated photovoltaic/thermal panel with the active cooling technique using Taguchi method, Energies 12 (6) (2019) 1022.